CTCF/cohesin organize the ground state of chromatin-nuclear speckle association

Ruofan Yu, Shelby Roseman, Allison P. Siegenfeld, Son C. Nguyen, Eric F. Joyce, Brian Liau, Ian Krantz, Katherine Alexander, Shelley L. Berger

Abstract

The interchromatin space in the cell nucleus contains various membrane-less nuclear bodies. Recent findings indicate that nuclear speckles, a distinct nuclear body, exhibit preferential interactions with chromatin in a ground state, potentially priming specific genes for speckle-mediated gene expression and induction. Key questions are how this preferred ground state of chromatin-nuclear speckle association is established and what are the gene regulatory roles of this layer of nuclear organization. We report that chromatin structural factors CTCF and cohesin are required for full ground association between DNA and nuclear speckles. Disruption of ground state DNA-speckle contacts via CTCF or cohesin depletion had minor effects on ground expression of speckle-associated genes, however we found strong negative effects on stimulus-dependent induction of speckle-associated genes. In contrast, disruption of the cohesin releasing factor WAPL, which stabilizes cohesin on chromatin, led to enhanced inducibility of speckle-associated genes. Thus, our findings support a role of ground state chromatin-speckle association in promoting gene inducibility. We also observed similar disruption of the chromatin-nuclear speckle association in cell lines derived from patients with Cornelia de Lange syndrome (CdLS), a congenital neurodevelopmental disease, in which cohesin pathways are involved, here revealing nuclear speckles as a new potential avenue of therapeutic inquiry. In summary, our findings uncover a novel mechanism underlying a new layer of regulation of chromatin organization and gene expression, mediated by chromatin-nuclear speckle association with relevance to human disease.

Introduction

Nuclear bodies, defined as membrane-less, morphologically distinct regions within the cell nucleus, have been implicated in chromosome organization(*1*) and gene regulation(*2*). One type of these nuclear structures are nuclear speckles, which consist mainly of RNA and proteins involved in numerous aspects of RNA expression, including transcription, splicing, polyadenylation, RNA modification and export(*3*). In recent years, evidence has emerged to propose an active role for nuclear speckles in gene regulation. For example, some viruses can utilize nuclear speckles to promote rapid production of mRNA(*4*), and, more generally, certain genes move closer to speckles in various biological processes such as heat shock(*5*), erythropoiesis(*6*), and p53 activation(*7*). Such increased chromatin-speckle association correlates with enhanced gene induction, potentially by bringing genes in close proximity to machinery of transcription, mRNA splicing, processing, and/or stabilization (*8*).

Several studies indicate that the ground chromatin-nuclear speckle association exhibits a similar pattern across different cell types (*9*, *10*). At ground state, regions proximal to nuclear speckles (compared to nuclear speckle distal regions) are depleted of heterochromatic markers Lamin and H3K9me3, while enriched of active markers H3K4me3 and H3K27ac; these regions also show higher gene density and overall higher gene expression levels (*9*, *11*). These findings suggest that association in the ground-state of nuclear speckles with chromatin may serve as a broad mechanism for gene regulation across various cell types. However, due to a lack of mechanistic knowledge of the factors that orchestrate ground-state chromatin-speckle association, the overall role of this layer of nuclear organization remains poorly understood.

Recent studies conducted in our lab demonstrate that the transcription factor p53, upon induced activity, facilitates interaction between a subset of its target genes and nuclear speckles(*7*). This discovery provides a mechanism, via transcription factor function, to promote inducible association between chromatin and nuclear speckles to boost gene expression. One notable observation was that p53 target genes located in close proximity to nuclear speckles prior to p53 activation are significantly more likely to increase association with speckles upon induction of the pathway (*7*). Previous studies also found that heat shock genes, which associate with speckles upon activation, are also pre-positioned at nuclear speckles (*5*). These findings highlight that gene regulation by DNA-speckle association is controlled on two levels: 1) conditional association upon change-of-state, which can be transcription factor mediated, and 2) ground association at the ground state, ground association at the ground state, which then informs conditional association of genes to move closer to speckles. In this study, we investigated the mechanism establishing the ground state of chromatin with nuclear speckles, its regulatory consequences, and its potential implication in a rare genetic disease, Cornelia de Lange syndrome.

Results

CTCF depletion leads to dissociation between chromatin and nuclear speckle

To discover factors involved in association between nuclear speckles and chromatin at ground state, our initial focus was to utilize computational approaches to identify factors that display enrichment in genomic regions associated with speckles. Genome-wide datasets of DNA associated with speckles were previously generated using SON TSA-seq, a technique that uses proximity labeling of DNA near to the structural nuclear speckle protein, SON (*7*, *9*, *10*). CTCF was reported to preferentially localize to chromatin associated with nuclear speckles [(*9*), and see Fig. 1A, 1B]. However, this observed enrichment could be due to CTCF's binding preference for active chromatin, which naturally tends to be in closer proximity to nuclear speckles compared to inactive chromatin. Indeed, we carried out correlation analysis of CTCF and found a genomic binding pattern that is comparable to the active chromatin marker H3K27ac, while showing an inverse relationship with the repressive marker H3K9me3 (Fig.1A, sample genomic regions shown in 1B). However, upon comparing the ChIP-seq profiles of CTCF, its binding partner cohesin subunit Rad21(*12*), and RNA Polymerase II (*13*), we discovered that CTCF and Rad21 exhibited greater similarity with SON than did PolII (Fig.1A,1B). This analysis indicates that enrichment of CTCF in speckle-associated DNA regions may surpass mere correlation with active chromatin.

To further test this hypothesis, we conducted a comparative analysis using a permutation test (*14*) to assess the degree of enrichment in speckle associated regions (SON-TSA-seq) for multiple euchromatic factors, including another chromatin structural protein YY1 (*15*), and transcription factors p53(*16*) and AP-1(*17*) in the fetal lung fibroblast cell line IMR90 (Fig. 1C) and other cell lines with available SON-TSA seq data (*7*, *9*, *10*) (Fig. 1D). We observed a notable and statistically significant enrichment of CTCF (Fig. 1C, left), supported by a high enrichment score (Z-score=10.276) and a minimal p-value. This was in stark contrast to lower enrichment scores for YY1, p53 and AP-1 (Fig. 1C, right panels). The results consistently demonstrated a pronounced and significant enrichment of CTCF binding sites within speckle-associated regions across various cell lines. This enrichment exceeded the other factors, suggesting that CTCF's presence in speckle-associated regions is unlikely solely attributable simply to its preferential positioning within active chromatin.

Given this correlative evidence, we next examined whether CTCF is necessary for association between chromatin and nuclear speckles. Utilizing a previously established auxin-inducible degron (AID) system in HeLa cells(*18*) (efficiency of CTCF knockdown demonstrated in Fig. S1A, B), we performed Oligopaint DNA-FISH(*19*) to visualize eight genes located at diverse positions on four distinct chromosomes, selected based on their varying nuclear speckle proximity. The level of association between each gene (DNA-FISH probes designed across a 50kb region centered on the transcription start site) and nuclear speckles is represented by the distance between FISH foci of corresponding genes and the closest nuclear speckle, labelled by immunofluorescence against speckle marker protein SON (*20*) (examples shown in Fig. 2A). We found that four genes located more proximal to nuclear speckles in the ground state (UTP18, SYMPK, GDF15 and POLH) showed dissociation between chromatin and nuclear speckle upon auxin induced degradation of CTCF for 24hr, while four genes located more distal to speckles in the ground state did not show changes in DNA-speckle distances (KCTD20, DDB2, CCL2, SESN1) (Fig. 2B). We noted that depletion of CTCF did not overtly impact nuclear speckle morphology in term of size (Fig. S1C, Speckle Area), shape (Fig. S1C, Eccentricity and Extent), nuclear size (Fig.S1C, Nuc. Area) nor average speckle count per nucleus (Fig. S1C, Speckle count). These results demonstrate that CTCF may facilitate association between chromatin and speckles, resulting in the preferential proximity of certain genes.

To further investigate the role of CTCF in the organization of DNA around nuclear speckles genome-wide, we performed Cut&Run of the major speckle component, SON (*20*). SON Cut&Run was employed to investigate the global association between chromatin and nuclear speckles, and is faster (2 days instead of 8-10 days) and relatively cost-effective compared to SON TSA-seq. The results exhibited a robust correlation with SON TSA-seq data, as observed in both the previously reported leukemia cell line K562 (*21*) and in our data obtained from IMR90 cells (Fig. S1D, SON TSA-seq data from (*7*)). To further evaluate the SON Cut&Run detection of chromatin-speckle association, we compared our SON Cut&Run to published large-scale multiplexed error-robust fluorescence *in situ* hybridization (MERFISH) data of speckles and DNA (*22*), also generated in IMR90 cells. We observed a clear inverse correlation between cytological distance between DNA and speckles measured by MERFISH and SON Cut&Run (Fig. S1E), indicating that genomic locations with high SON Cut&Run signal are closer to nuclear speckle and vice versa. Oligopaint DNA-FISH of specific genes performed in our study also showed a similar inverse correlation (Fig. S1F). Taken together, these data establish SON Cut&Run as a valid technique for genome-wide measurement of DNA-nuclear speckle association.

We then utilized SON Cut&Run to profile the effect of reducing CTCF levels on gene-speckle association genome-wide. We used two approaches: (1) primary lung fibroblast IMR90 cells with 48 hr siRNA knockdown against CTCF and (2) HeLa cells with 24 hr auxin inducible degradation of CTCF. In both systems, an overall decrease of SON signal was detected in large regions that were speckle associated in the control condition (sample regions shown in Fig. 2C, and whole Chromosome 1 view in Fig. S1G). Of note, these SON enriched regions were termed speckle-associated domains (SPADs) and spans large genomic distances of Megabases(*9*). At single gene loci, the change in SON Cut&Run intensity upon CTCF depletion was also confirmed (Fig. 2D compared to Fig. 2B). In further analysis, we examined changes in SON intensity within SPADs and identified a substantial decrease in SON levels across SPADs in both cell lines (Fig. 2E and F). To better characterize the change in SON signal with regard to CTCF positioning, we analyzed SON signal level across all CTCF genomic binding sites within IMR90 cells and observed a drastic decrease upon siRNA mediated CTCF knockdown (Fig. 2G). To further explore CTCF's role in speckle association across cell types, a third system was utilized.

Here, HaloTAG-labeled CTCF underwent 32-hour degradation via HaloPROTAC3 in HCT116 colorectal carcinoma cells. We again observed an overt decrease of SON signal across CTCF binding sites upon CTCF depletion (Fig. 2H). Taken together, these findings support an important role of CTCF in mediating the ground state of association between chromatin and nuclear speckles across multiple cell types.

CTCF-cohesin interaction is necessary for chromatin-nuclear speckle association

One of the most intensively characterized functions of CTCF is the anchoring of the cohesin complex. Over 90% of CTCF DNA-binding sites across the genome overlap with cohesin (*23*), and CTCF is known to stabilize cohesin on chromatin (*24*). CTCF binds to the genome through its zinc finger motif, and associates with Rad21 and SA1/2 proteins through its N-terminal region, facilitating the stabilization of cohesin at specific genomic sites (*12*, *23*). Cohesin is loaded onto genome by the NIPBL/MAU2 complex (*25*), where it binds to DNA in a ring-shaped structure consisting of SMC1 and SMC3(*26*), and is subsequently released from DNA by the cohesin unloader WAPL. To evaluate whether the N-terminal domain of CTCF was important for nuclear speckle contacts, we constructed N-terminal deletion (1-266) and C-terminal deletion (576-727) mutations in a transient expression plasmid with FLAG-tagged CTCF. This construct was transfected into the HeLa-CTCF-AID cell line and treated with auxin to deplete endogenous CTCF, so that exogenous CTCF will predominate. To assay how each CTCF mutant affected chromatin-speckle association, we utilized two probes targeting the speckle proximal genes UTP18 and POLH; both genes showed significant dissociation from speckles after 24 hours of auxin induced CTCF degradation (see Fig. 2B). DNA-FISH showed that both wildtype (WT) and C-terminal deleted CTCF (CTD) constructs were functional in maintaining speckle proximity of UTP18 and POLH (Fig. 3A, B), the while CTCF N-terminal deletion (NTD) was not able to maintain speckle proximity. Hence, the N-terminus of CTCF, which is required for direct interaction with cohesin, is also required for speckle association, whereas the C-terminus, which does not directly interact with cohesin, is not involved in speckle association, indicating the cohesin has a potential role in mediating chromatin-speckle association.

Given the implication that CTCF-Rad21 interaction is important, we investigated whether acute depletion of cohesin subunit Rad21 would dissociate chromatin from nuclear speckles. We utilized a Rad21-AID system in HeLa (*18*), where endogenous Rad21 is degraded rapidly (within 1hr) after auxin treatment (Fig.S2A, B). Similar to CTCF depletion (Fig. S1C), we found no overt change in nuclear speckle morphology with Rad21 degradation (Fig. S2C). DNA-FISH indicated that genes located in close proximity to nuclear speckles at ground state exhibited significant dissociation between chromatin and nuclear speckles following acute depletion of Rad21, while genes further away from speckle did not (Fig. 3C); these data closely matched the CTCF depletion (see Fig. 2B).

SON Cut&Run experiments also showed that upon Rad21 depletion, SPADs showed global reduction of chromatin-speckle association (Fig. 3D, E, whole Chromosome 1,2 view in Fig. S2D). Further, siRNA knockdown of cohesin subunits STAG1 and STAG2, responsible for bridging CTCF-cohesin interaction(*12*), led to dissociation of the speckle proximal UTP18 gene (Fig. 3F, upper), but not the speckle distal KCDT20 gene (Fig. 3G, upper). Collectively, these results implicate the importance of the cohesin complex cooperating with CTCF in organizing chromatin around nuclear speckles.

Our findings strongly suggest that the loss of CTCF/cohesin results in a decrease in the ground state chromatin-nuclear speckle association. To further test this hypothesis, we investigated whether, in contrast, gain of CTCF/cohesin leads to increased chromatin association with nuclear speckles.

Cohesin bound to chromatin is unloaded by the releasing factor WAPL (*27*), hence, disruption of WAPL stabilizes cohesin binding on genome and antagonizes cohesin depletion (*28*). We utilized siRNA knockdown of WAPL in HeLa cells and performed DNA-FISH. Interestingly, we found no apparent change in gene-speckle distance of speckle proximal gene UTP18 (Fig.3F, upper). In contrast, the speckle distal gene KCTD20 showed increased speckle association in WAPL KD cells (Fig. 3G, upper). Subsequent SON Cut&Run experiments also corroborated DNA-FISH results of these two genes (Fig. 3F, G, lower panels). While WAPL KD did not lead to apparent change in SON signal intensity across ground SPADs of control HeLa cells (Fig. 3H), however, the size of SPADs under the two conditions showed significant widening of SPADs in the WAPL KD cells (Fig. 3I, sample regions showed in Fig. 3J, whole Chromosome 1,2 view in Fig. S2E). Reciprocal analyses also demonstrated higher SON signal intensity across SPADs in WAPL KD cells comparing to control cells (Fig. S3F). Collectively, these findings indicate that the stabilization of cohesin through WAPL reduction expands the genomic regions associated with speckles.

Disruption of nuclear speckle association hinders the induction of nuclear speckle proximal genes

Previous studies have established a consensus that highly expressed genes often tend to be located in close proximity to nuclear speckles (*9*, *10*, *29*). In line with this observation, our gene ontology (GO) analysis of genes located in close proximity to speckles in both IMR90 and HeLa cells (genes with top 10% highest SON Cut&Run signal) revealed significant enrichment of essential biological processes. These processes included gene expression and various pathways associated with macromolecule biosynthesis (Fig. 4A). The association between nuclear speckle and chromatin, shown in analyses above to be dependent on CTCF and cohesin, may thus be of vital importance specifically in regulating these molecular pathways.

Previous studies show that CTCF(*30*) and cohesin perturbation (*31*, *32*) impair activation of a subset of genes, and, importantly, both factors are essential as disruption of either can lead to developmental failure or cell death (*33*–*35*). In contrast, disruption of either CTCF or cohesin do not cause a broad change in steady state gene expression(*36*–*38*). Similarly, our RNA-seq of cells altering CTCF, Rad21 or WAPL levels also showed only moderate changes of steady state gene expression (Fig.S3A-C). However, when we grouped the transcriptome based on gene distance to speckles, we observed a small yet significant downregulation of genes proximal to speckles in HeLa cells with auxin induced degradation of CTCF or Rad21 (Fig. 4B, C), indicated a potential role in facilitating the expression of genes located in proximity to nuclear speckles, which were previously demonstrated (Fig. 4A) to be enriched in various vital biological processes.

Nuclear speckles are proposed to facilitate gene induction under various external stimuli (5, 7). Similarly, CTCF loss-of-function is more consequential for gene expression upon change of state (30, 38). Thus, given the modest consequences of CTCF/cohesin perturbation on speckle associated gene expression at steady state (Fig. 4B, 4C), we next investigated gene activation under stress to determine whether CTCF/cohesin facilitates induction of speckle-proximal genes. We used heat as a stimulus, as heat shock is well-known to induce numerous protective genes including protein chaperones and DNA damage repair genes (*39*). We subjected HeLa cells to a heat shock of 1hr at 45 °C and detected induction of heat shock response genes in RNA-seq (Fold change >0 and p<=0.01, volcano plot in Fig. S3D). Using DESeq2(*40*), we performed interaction analysis to examine the heat shock-specific effect of CTCF reduction on genes with diverse speckle proximity. All genes with significantly different

induction level ($p<0.05$) were assigned to three bins, distal, medial, and proximal, based on SON Cut&Run signal. In line with our hypothesis, we found that CTCF depletion resulted in a drastic decrease in heat shock-dependent induction of speckle proximal genes compared to speckle distal gene, both in overall level (represented by Log2 fold change, Fig. 4D left) and number of differentially induced genes within each bin (Fig. 4D right).

Reciprocally, we identified genes with significantly differential SON Cut&Run signal upon CTCF KD (as in (*7*)). Notably, genes that moved away from nuclear speckles (exhibiting decreased SON Cut&Run signal) showed lower induction both in terms of level (Fig. 4E) and number (Fig. 4F, example genes shown in Fig. 4G) compared to genes that moved towards nuclear speckles. These findings indicate that, in response to heat shock, CTCF disruption has a heightened impact on the induction of genes located near nuclear speckles during heat shock. Furthermore, increased proximity to nuclear speckles positively influences overall gene induction.

Another instance of gene regulation by nuclear speckle association is the gene activation by the p53 stress-responsive transcription factor (*7*). We assayed gene induction level in IMR90 cells with nutlin-3a treatment for 6 hours to activate p53 signaling pathway (*7*). We found that similar to heat shock in HeLa cells, siRNA mediated CTCF KD led to a significant reduction of speckle proximal gene induction comparing to speckle distal genes (Fig. 4H). Genes with decreased nuclear speckle association displayed reduced induction in both expression level (Fig. 4I) and quantity (Fig. 4J, example genes shown in Fig. 4K), in contrast to genes with increased nuclear speckle association.

To further corroborate the role of nuclear speckle proximity in gene induction, we compared RNA-seq results of heat-shocked HeLa cells with siRNA knockdown of a negative control or WAPL, predicting that WAPL KD will increase gene expression correlating with closer proximity to speckles. Consistently, we found that genes relocating towards nuclear speckles exhibited higher levels of overall induction (Fig. 4L). Additionally, the majority of significantly more induced genes were those moving closer to speckle proximity (Fig. 4M, example genes shown in Fig. 4N). Taken together, these findings provide compelling evidence that, upon stimulation of a gene pathway, CTCF/cohesin-mediated speckle association acts to amplify induction of genes located in close proximity to speckles (Fig. 4O).

Chromatin-speckle dissociation presents in CdLS patient derived cell lines with mutation of Rad21 genes

Given the proposed roles of CTCF and cohesin in mediating association between chromatin and nuclear speckles, an intriguing question arises as to whether disease-associated mutations could alter DNA-speckle association. Variations in cohesin component RAD21(*41*) and SMCs (*42*), and in the cohesin loading factor NIPBL(*43*) are causative for Cornelia de Lange Syndrome (CdLS), an autosomal dominant developmental disorder occurring in one per ten thousand births. CdLS is characterized by intellectual disability, gastrointestinal disorders, and congenital heart defects (*44*). Although cohesin is vital for sister chromatid cohesion and cell cycle progression, structural chromatin defects are not overt in CdLS patient-derived cell lines (*45*, *46*). Since altered gene expression occurs in various models of cohesin mutations, developmental deficits in CdLS are proposed to arise from changes in gene expression, however, the mechanism is not fully understood (reviewed in *47*).

Given our findings of cohesin maintaining DNA-speckle association and gene regulation, we investigated whether CdLS-linked mutations in Rad21 disrupt DNA-speckle association correlating with reduced gene induction. We utilized a CdLS patient derived Lymphoblastoid cell line (LCLs) bearing a duplication within the 5th exon of Rad21: c.592_593dup; p. (Ser198Argfs*6); this mutation causes a

proximal premature stop codon that likely leads to nonsense mediated decay of the mutated transcript (*47*). We confirmed this genomic mutation by Sanger sequencing (Fig. S4A), and with RNA-seq showing ~50% reduction of Rad21 transcript (Fig. S4B). Similar to cells bearing CTCF and Rad21 KD shown above (Fig. S1C and Fig. S2C), nuclear speckle morphology did not change overtly in patient LCL (P561) compared to LCLs derived from two healthy individuals (Fig. 5A, S4C). SON Cut & Run on patient derived LCLs revealed a striking reduction of genome-wide SON signal (Fig. 5B, C, whole chromosome 1 view in Fig. S4D), indicating global dissociation between chromatin and nuclear speckle similar to CTCF or Rad21 knockdown in HeLa or IMR90 cells.

To examine the effect of Rad21 mutation on gene induction, we heat-stressed patient-derived LCL cells for 1 hour and performed RNA-seq. Similar to CTCF disruption in HeLa and IMR90 cells shown in Fig. 4, a notable decrease in the induction of genes located near speckles was observed in P561 compared to Ctrl1 (Fig. 5D), whereas the differential gene induction status between two control cell lines did not exhibit a clear correlation with nuclear speckle proximity (Fig. S4E). Additionally, genes with reduced speckle association in P561 were significantly less induced compared to genes with increased speckle association (Fig. 5E). Among the genes exhibiting reduced induction, notable examples are the molecular chaperone gene HSP90AB1(*48*) and stem loop binding protein SLBP (*49*) which is necessary for pre-mRNA processing of histone mRNA (Fig. 5F). Collectively, the disruption of CTCF/cohesin not only consistently affects the ground association between chromatin and speckles but also impairs the complete induction of speckle proximal genes, not only in laboratory cell lines but also in cell lines derived from individuals with CdLS.

Discussion

In this study, we present evidence supporting a new function of chromatin structural factors CTCF and cohesin in mediating the ground state of chromatin-speckle association (Fig. 5G). We found that disruption of CTCF or cohesin led to genome-wide dissociation between chromatin and nuclear speckles, and significantly impaired inducibility of genes located proximal to speckles. Importantly, this effect was consistent across various cell lines. We propose that chromatin-speckle association positions and thus primes genes for further conditional chromatin-speckle association under various stimulation, thereby amplifying expression of nuclear speckle-proximal genes upon induction. Moreover, we observed a similar disruption of chromatin-speckle association and impairment of gene induction in a cell line derived from a patient with Cornelia de Lange Syndrome, which notably involves Rad21 deficiency, thus indicating that dysfunction of chromatin-speckle association occurs in human disease.

Our results provide a new perspective on gene regulatory roles of CTCF and cohesin. This is of particular importance, considering that disruption of these factors does not induce drastic changes in the transcriptome under steady-state conditions (*36–38*). Rather, we find that depletion of CTCF and cohesin lead to impaired gene induction under various ‘change-of-state’ conditions, such as heat-shock and p53 activation, and our results point to this transcriptional effect as an outcome of their critical function in establishing the ground state of chromatin-nuclear speckle association. Hence, we propose that CTCF/Rad21 setting up this ground state functions as an additional regulatory mechanism to further boost gene expression in response to stimuli in conjunction with canonical pathways.

Both CTCF and Rad21 have established roles in facilitating chromatin loop formation. Consequently, further investigation is required to explore the relationship between nuclear speckles and chromatin conformation. It has been reported that nuclear speckle-associated chromatin shows enrichment in the A1 active subcompartment, and disruption of speckle protein SRRM2 reduces

chromatin interactions in A1 (*50*). On the other hand, a recent study has reported minimal impact on chromatin loop formation upon disruption of nuclear speckles (Personal communication). These findings underscore the need for continued research to unravel the intricate interplay between nuclear speckles and the broader landscape of 3D chromatin organization.

Nuclear speckles have been extensively proposed to play a crucial role in facilitating gene expression (*5*, *7*, *8*). Despite the abundance of evidence supporting the correlation between speckle proximity and gene expression levels, a significant limitation in the field has been the absence of causative evidence due to the essential nature of speckle components, such as SON and SRRM2 (*20*). This study provides compelling evidence showcasing the detrimental effect of CTCF/cohesin disruption on the association between chromatin and nuclear speckles, resulting in impaired induction of genes located in close proximity to speckles, while having minimal impact on genes distantly located from speckles (Fig. 4). These findings represent the first direct evidence substantiating the pivotal role of nuclear speckle association in facilitating overall gene induction.

Our observations, in conjunction with previous studies, underscores the significance of nuclear speckles as vital hubs for genes that necessitate high and/or rapid induction. Disruption of this hub could lead to aberrant gene expression patterns and potentially contribute to disease outcome. Our findings highlight the role of Rad21 variation in causing speckle dissociation and impairing gene induction in CdLS patient-derived cells (Fig. 5). Moreover, multiple reports have implicated mutations within nuclear speckle components, including SON (*51*) and SRRM2 (*52*), in neurodevelopmental diseases. Further exploration of nuclear speckles could thus shed light on the molecular mechanisms underlying gene dysregulation in diseases and uncover potential therapeutic targets.

Materials and Methods

1. Experimental methods

a. Cell culture and gene knockdown

HeLa CTCF-AID and HeLa Rad21-AID acquired from () were grown in DMEM high glucose 4.5 gm/L - no sodium pyruvate (Corning, 10-017-CM) supplemented with 10% fetal calf serum and 1% Penn/Strepp. CTCF knockdown was induced by 24 hours of 500uM Indole-3-acetic acid sodium (Sigma-Aldrich I5148), and control cells treated with 0.1% DMSO unless otherwise noted. siRNA targeting either WAPL (siRNA 148512, AM16708, ThermoFisher) or negative control (AllStars Negative Control siRNA, QIAGEN) was transfection with DharmaFECT (FisherScientific, T-2001-02) according to manufacturer protocol and incubated for 48 hours prior to harvesting.

Passage 25-35 IMR90 primary lung fibroblast cell line acquired from ATCC (Cat#CL186) were grown in DMEM (ThermoFisher) supplemented with 10% fetal calf serum and 1% Penn/Strepp. siRNA targeting either CTCF (Hs_CTCF_6 FlexiTube siRNA, QIAGEN) or negative control (AllStars Negative Control siRNA, QIAGEN) was transfection with DharmaFECT (FisherScientific, T-2001-02) according to manufacturer protocol and incubated for 48 hours prior to harvesting.

HCT116 HaloTAG-CTCF cells were cultured in McCoy media (Thermo Fisher Scientific, 16600082) with 10% FBS (Peak Serum, PS-FB2) and 1%Penn/strepp (Life Technologies, 15070063). CTCF knockdown was induced for 32 hours with HaloPROTAC3 (330nM, AOBIOUS AOB36136) or DMSO control (0.1% DMSO).

Lymphoblastoid cell lines were cultured in RPMI 1640 with 2mM L-glutamine (Invitrogen, 11875085) supplemented with 20% fetal calf serum and 1% Penn/Strepp.

b. Western blotting and antibodies

Samples were lysed with RIPA buffer (150nM NaCl, 1% IGEPAL, 0.5% sodium deoxycholate, 0.1% SDS and 50mM Tris pH7.4). Protein concentration was determined by bicinchoninic acid assay (BCA) protein assay (#23227, Life Technologies). Samples were separated using precast 4-12% Bis-Tris polyacrylamide gels (ThermoFisher Scientific, NP0321BOX) in the presence of SDS. Proteins were transferred to nitrocellulose membrane, blocked with 5% milk TBST and probed with the following primary antibodies: 1. Anti-CTCF antibody (1:5000, abcam, ab188408); 2. Anti-Rad21 antibody (1:1000, Cell Signaling, 4321s); 3. Anti-GAPDH antibody (1:1000, Cell Signaling, 5174); 4. Anti-H3 antibody (1:2500, abcam, ab1791), and secondary goat anti rabbit antibody (1:10000, Bio-Rad, 1706515). Chemiluminescent detection of immunoblots was performed using Thermo Scientific SuperSignal West Pico PLUS Chemiluminescent Substrate (ThermoFisher Scientific, 34577).

c. Immunofluorescence and antibodies

Cells were washed twice with PBS and fixed with Paraformaldehyde solution 4% in PBS (Santa Cruz Biotechnology, CAS 30525-89-4) for 10 minutes at room temperature, washed again with PBS (Corning, 21-031-CV) then permeated with 0.1% PBS Triton X-100 for 15 minutes. Cells were incubated overnight in primary antibodies targeting GFP (Roche, 11814460001) or SON (abcam, ab121759) diluted 1:200 in PBS at 4C. Secondary antibody conjugated with Goat anti-Rabbit IgG Alexa Fluor™ 488 (ThermoFisher Scientific, A-11008) and Goat anti-Mouse IgG Alexa Fluor™ 647 (ThermoFisher Scientific, A-21235) were diluted 1:200 in PBS and used respectively. After 1 hour incubation at room temperature, samples were washed and incubated in 1:10000 DAPI (Invitrogen, D1306, 5 mg/mL) for

5min. All imaging in this study was performed with Nikon Eclipse Ti2 widefield microscope. For IF only experiments, cells were imaged at focal plane with a 60x oil-immersion objective, and a deep depletion CCD camera cooled to between -70 and -80C.

d. ImmunoDNA-FISH

Cells were treated with same protocol as immunofluorescence. After secondary antibody incubation, slides were fixed with 4% PFA in PBS for 10 minutes at room temperature, washed with PBS and permeabilized with 0.5% Triton in PBS for 15 minutes. Subsequently, DNA-FISH was performed as described (Nguyen and Joyce, 2019). Oligopaint DNA-FISH probes to target genes were designed across a 50kb region centered on the transcription start site as described (Petrovic et al., 2019). Cells were imaged in a series of 28 optical sections spaced 0.286 microns apart with a 60x oil-immersion objective and a deep depletion CCD camera cooled to between -70 and -80C.

e. SON Cut & Run

SON Cut & Run were performed based on protocol described with minor modification (). For each experiment, a total 600K trypsinized cells were harvested, underwent nuclear isolation then incubated with 40ul of concanavalin A lectin beads (BioMag Plus, BP531) for 10 minutes. Beads bound cells were evenly split into 2 tubes and incubated overnight at 4C in 1:100 Anti-SON (abcam, ab121759) or Rabbit Anti-Mouse IgG Antibody (Millipore, 06-371). Subsequent DNA was extracted and purified by PCI-chloroform Alcohol and ethanol precipitation. Resulting DNA were prepared for sequencing using the NEBNext Ultra II DNA Library Prep Kit for Illumina (NEB, E7645L). Library sizes were determined by Bioanalyzer, and concentration determined using NEBNext Lib Quant Kit (NEB, E7630). Libraries were sequenced with an Illumina NextSeq550 with 42bp per read (total of 84bp) using the NextSeq 500/550 High Output 75-cycle v2.5 kit (Illumina, 20024906) reads at a sequencing depth of approximately 30 million reads per sample.

f. SON Cut & Tag

SON Cut&Tag was performed according to the published protocol by Kaya-Okur et al. (2019) with minor modification. For each experiment, 1 million cells were harvested, washed and lysed on ice for 10 minutes. Nuclei were resuspended in PBS and fixed with 0.1% formaldehyde for 2 minutes at room temperature and quenched with 75mM glycine. 250,000 nuclei per condition (as determined by a hematocytometer) were used per condition. Samples were incubated with 1:50 of anti-SON antibody (abcam, ab121759) and incubated 4C overnight. The beads were then resuspended in secondary antibody in wash buffer (1:100 guinea pig anti-rabbit ABIN101961) and nutated at room temperature for 1 hour. DNA was purified by PCI-chloroform extraction. The purified DNA was then amplified by PCR using NEBNext HiFi 2x PCR Master Mix (NEB M0541S), and the resulting library was purified using 1.3X SPRI purification (Omega Bio-Tek, M1378-01). Libraries were sequenced using a NextSeq1000 (Illumina) with 50bp paired end reads at a sequencing depth of approximately 10-20 million reads per sample.

g. Plasmid construction and transfection

Plasmid mutagenesis was performed on pKS070 - pCAGGS-3XFLAG-(human) CTCF-eGFP (Addgene Plasmid #156448) for CTCF and mEmerald-Rad21-N-18 (Addgene Plasmid #54248) for Rad21. Mutagenesis was carried out with QuikChange II Site-Directed Mutagenesis Kit (Agilent, 200523) with primers listed below.

Plasmid transfection was carried out with XtremeGENE HP (Millipore Sigma, 6366244001) according to manufacturer protocol at a reagent/DNA ratio of 2:1 in serum free media. Cells

were incubated in transfection mixture for 4 hours then changed to regular media, followed by designated treatments the next day.

CTCFnterm_F2	CAGTGTGAGCTTTGCAGT
CTCFnterm_R2	ACCGGTCTTATCGTCATC
CTCFcterm_F2	CTTAAGGGGGGAGCAGGA
CTCFcterm_R2	ACAATTATCAGCATGTCTTGCC
RAD2115DEL_F	ACCATGACTGATCAAACAAC
RAD2115DEL_R	CCCACCCATTGATACATTATC

h. Polyadenylated RNA-seq

Cells were lysed in TRIzol (15596018, Thermo Fisher Scientific) and snap frozen. RNA was then isolated using chloroform extraction, followed by QIAGEN RNeasy Mini Kit isolation (#74106), including DNA digestion with DNase. Poly(A)+ RNA was further isolated using double selection with poly-dT beads (E7490, NEB). RNA-seq libraries were prepared using the NEBNext Ultra II Directional Library Prep Kit for Illumina (E7760, NEB). The size of the libraries was determined using a Bioanalyzer, and their concentration was determined using the NEBNext Lib Quant Kit (E7630, NEB). The libraries were sequenced on an Illumina NextSeq 550, utilizing paired-end sequencing with 42 bases per read, at a sequencing depth of approximately 15 million reads per sample.

2. Data processing and analysis

a. ChIP-seq correlational and permutation analysis

Spearman correlation in 1A was calculated by deepTools *multiBigwigSummary* with -bs of 50000. All previously published genomic resources used in this study are listed in Table S.

Permutation analysis in 1C was performed as follow: 1. List of predicted binding target genes of designated factors were retrieved from Transcription Factor Gene Database (https://tfbsdb.systemsbiology.net/). Motif list used are listed as follow, CTCF: CTCF_C2H2_full_monomeric; YY1: YY1_C2H2_full_monomeric; p53: Tp53_p53l_DBD_dimeric; AP1: V_AP1_01_M00517. 2. Genomic coordinates of target gene list spanning +50kb and -50kb of transcription start site (TSS) were used as query due to the broad distribution of SON signal across the genome. 3. Permutation tests with RegioneR (https://bioconductor.org/packages/release/bioc/html/regioneR.html) were performed using genomic regions spanning 50 kilobases upstream and downstream of all hg19 RefSeq gene transcription start sites as the background (universe), *with randomize. function= resampleRegions, evaluate.function=meanInRegions*, and randomize time *n=1000*.

b. Immunofluorescence (IF) data processing and analysis

All IF images were taken at the focal plane with the autofocus function of Nikon NIS software on a Nikon Eclipse Ti2 widefield microscope with a 60x oil-immersion objective lens. Subsequent image processing was performed with CellProfiler (https://cellprofiler.org/) to identify nuclear speckle and measure various size and shape parameters. Pipeline and notes are available on Github:
https://github.com/Chalietia/CellProfiler/blob/main/SpeckleSPEC1.1.cppipe

c. ImmunoDNA-FISH data processing and analysis

For All ImmunoDNA-FISH, cells were imaged in a series of 28 optical sections. Resulting image stacks were first maximum projected with *MakeProjection* function of CellProfiler. All DNA-FISH foci within DAPI stained nucleus were identified, nucleus with more than 4 identified FISH foci were removed. After identifying nuclear speckle, the distance between center of FISH foci and the edge of its nearest nuclear speckle was measured in pixel. In subsequent post-processing, pixel distance* 0.11 um/pixel was calculated as the final physical distance. Pipeline, QC and sample data are available on https://github.com/Chalietia/CellProfiler. Speckle distance distribution p values were calculated using Mann-Whitney-Wilcoxon tests.

d. SON Cut&Run/SON Cut&Tag data processing

Sequencing reads were aligned to human reference genome assembly GRC37/hg19 with the following parameter using Bowtie2 (http://bowtie-bio.sourceforge.net/bowtie2/index.shtml): --local --end-to-end --very-sensitive --no-mixed --no-discordant --phred33 -I 10 -X 1000- x hg19, subsequently filtered with samtools view -q 5 and deduplicated with Picard (https://broadinstitute.github.io/picard/). According to ours and previous observation (), SON signal across genome is broad and not as highly enriched as regular transcription factors. Therefore, to minimize the impact of noise, sharp peaks were called for all bam files by macs3 callpeak -f BAM -g 2.7e9 -q 0.1. The noise peaks have an average size of 200bp and cover less than 0.2% of the effective genome. Combined noise peaks files were then merged with ENCODE hg19 blacklist (https://github.com/Boyle-Lab/Blacklist/blob/master/lists/hg19-blacklist.v2.bed.gz) and excluded from all subsequent analysis. For all results except CTCF binding region visualization in Fig. 2G-H, Bigwig and BedGraph files were generated with deepTools: bamCompare -b1 $SON -b2 $IGG -bs 5000 --smoothLength 15000 --effectiveGenomeSize 2864785220 --exactScaling --normalizeUsing RPKM --scaleFactorsMethod None -bl blacklistPEAK.merge.bed. For Fig. 2G-H, given the narrower nature of CTCF binding peaks, Bigwig files were generated with -b $SON -bs 50 --effectiveGenomeSize 2864785220 --exactScaling --normalizeUsing RPKM.

e. SON Cut&Run QC

For correlation between SON TSA-Seq and SON Cut&Run, average IGG normalized SON signal from both experiments was calculated and compared across CDS of all RefSeq genes.

For comparison between MERFISH and SON Cut&Run, MERFISH data containing location and distance between probes and nearest nuclear speckle was retrieved from https://zenodo.org/record/3928890. Average IGG normalized SON signal at corresponding genomic loci was calculated and compared. Top 5% most distant loci in MERFISH data were considered as outlier and excluded from this analysis.

For comparison between ImmunoDNA-FISH and SON Cut&Run, average IGG normalized SON signal from TSS -25kb to TSS +25kb of corresponding genes was calculated and compared. This region is where the Oligopaint DNA-FISH probes were located.

f. Speckle associated domains (SPADs) calling

SPAD calling was performed by SICER (https://pubmed.ncbi.nlm.nih.gov/24743992/) with the following parameters: sicer -t $SON -c $IGG -s hg19 -fdr 0.1 -w 2000 -g 20000. To identify consensus regions, SPADs identified from two technical replicates for each condition were intersected as final output.

g. SON Cut&Run differential analysis

SON Cut&Run differential analysis was based on previously published method (, stepwise instruction available https://github.com/katealexander/TSAseq-

Alexander2020/tree/master/genomicBins_DiffBind) with minor modification. Briefly, with deduplicated bam files, SON signal was quantified over sliding windows of 50kb (slid by 1/10th of the window size) using DiffBind with input subtraction (). Blacklist files generated in (d) were used. Normalization method was set to DBA_NORM_RLE. Regions with significant increase or decrease of SON signal were separated into different files, and those regions with fdr<0.1 was considered as differential and merged with BEDTools as differential domains. Genes located within differential domains were extracted with an in-house Python script.

h. Gene ontology (GO) analysis
Genes exhibiting the highest 10% SON Cut&Run signal across coding sequences (CDS) in both IMR90 and HeLa cells were selected as input for the GO Biological Process analysis with default setting on STRING database (http://string-db.org). Resulting GO categories with strength>0.2, fdr<0.01, and a background 100 to 3000 genes were subjected to REVIGO (http://revigo.irb.hr/) analysis to identify non-overlapping clusters. The GO terms with largest background within each cluster were selected for visualization.

i. RNA-seq data processing
RNA-seq data was aligned to the reference human genome assembly, GRC37/hg19, using the splice-aware STAR alignment (https://github.com/alexdobin/STAR/releases) with the following settings: --outFilterType BySJout --outFilterMultimapNmax 20 --alignSJoverhangMin 8 --alignSJDBoverhangMin 1 --outFilterMismatchNmax 999 --outFilterMismatchNoverReadLmax 0.04 --alignIntronMin 20 --alignIntronMax 1000000. Reads for each gene with RefSeq annotations were counted using htseq-counts (). Normalized counts and differential analysis were generated with Deseq2 (). Statistical differences between log2FC in different SON signal bins were determined using Mann-Whitney-Wilcoxon tests.

j. RNA-seq interaction analysis
Interaction analysis was performed based on Deseq2 instruction (https://www.bioconductor.org/packages/devel/bioc/vignettes/DESeq2/inst/doc/DESeq2.html#interactions), with the following design: design= ~genotype + condition + genotype: condition. To specifically look at how condition effect (e.g., heat shock) differ across genotype (e.g., CTCF KD), the interaction term were extracted with results (dds, name="genotypeII.conditionB"). All genes with a p value <0.05 were considered to have significantly differential conditional effect.

3. Genomics data reference

All previously published data used in this study is listed below:

Figure	Description	Identifier
1A,1B	IMR90 H3K9me3	ENCFF144BLD
	IMR90 RNAPolII	GSM4586500
	IMR90 SON-TSA-seq	GSE154095
	IMR90 H3K27ac	GSM3985197
	IMR90 RAD21	GSM3985205

	IMR90 CTCF	GSM3985197
	IMR90 RNAseq	GSE139003
2G	CTCF all peak IMR90	ENCSR000EFI
2H	CTCF all peak HCT116	GSE217760
S1D	IMR90 SON-TSA-seq	GSE154095

References

1. S. A. Quinodoz, N. Ollikainen, B. Tabak, A. Palla, J. M. Schmidt, E. Detmar, M. M. Lai, A. A. Shishkin, P. Bhat, Y. Takei, V. Trinh, E. Aznauryan, P. Russell, C. Cheng, M. Jovanovic, A. Chow, L. Cai, P. McDonel, M. Garber, M. Guttman, Higher-Order Inter-chromosomal Hubs Shape 3D Genome Organization in the Nucleus. *Cell*. **174**, 744-757.e24 (2018).

2. M. Morimoto, C. F. Boerkoel, The Role of Nuclear Bodies in Gene Expression and Disease. *Biology*. **2**, 976–1033 (2013).

3. D. L. Spector, A. I. Lamond, Nuclear Speckles. *Csh Perspect Biol*. **3**, a000646 (2011).

4. A. Mor, A. White, K. Zhang, M. Thompson, M. Esparza, R. Muñoz-Moreno, K. Koide, K. W. Lynch, A. García-Sastre, B. M. A. Fontoura, Influenza virus mRNA trafficking through host nuclear speckles. *Nat Microbiol*. **1**, 16069 (2016).

5. J. Kim, N. C. Venkata, G. A. H. Gonzalez, N. Khanna, A. S. Belmont, Gene expression amplification by nuclear speckle association. *J Cell Biology*. **219**, e201904046 (2019).

6. J. M. Brown, J. Green, R. P. das Neves, H. A. C. Wallace, A. J. H. Smith, J. Hughes, N. Gray, S. Taylor, W. G. Wood, D. R. Higgs, F. J. Iborra, V. J. Buckle, Association between active genes occurs at nuclear speckles and is modulated by chromatin environment. *J Cell Biology*. **182**, 1083–1097 (2008).

7. K. A. Alexander, A. Coté, S. C. Nguyen, L. Zhang, O. Gholamalamdari, P. Agudelo-Garcia, E. Lin-Shiao, K. M. A. Tanim, J. Lim, N. Biddle, M. C. Dunagin, C. R. Good, M. R. Mendoza, S. C. Little, A. Belmont, E. F. Joyce, A. Raj, S. L. Berger, p53 mediates target gene association with nuclear speckles for amplified RNA expression. *Mol. Cell*. **81**, 1666-1681.e6 (2021).

8. P. Bhat, A. Chow, B. Emert, O. Ettlin, S. A. Quinodoz, Y. Takei, W. Huang, M. R. Blanco, M. Guttman, *bioRxiv*, in press, doi:10.1101/2023.01.04.522632.

9. Y. Chen, Y. Zhang, Y. Wang, L. Zhang, E. K. Brinkman, S. A. Adam, R. Goldman, B. van Steensel, J. Ma, A. S. Belmont, Mapping 3D genome organization relative to nuclear compartments using TSA-Seq as a cytological ruler. *J. Cell Biol.* **217**, 4025–4048 (2018).

10. L. Zhang, Y. Zhang, Y. Chen, O. Gholamalamdari, Y. Wang, J. Ma, A. S. Belmont, TSA-seq reveals a largely conserved genome organization relative to nuclear speckles with small position changes tightly correlated with gene expression changes. *Genome Res*. **31**, 251–264 (2021).

11. Y. Wang, Y. Zhang, R. Zhang, T. van Schaik, L. Zhang, T. Sasaki, D. Peric-Hupkes, Y. Chen, D. M. Gilbert, B. van Steensel, A. S. Belmont, J. Ma, SPIN reveals genome-wide landscape of nuclear compartmentalization. *Genome Biology*. **22**, 36 (2021).

12. Y. Li, J. H. I. Haarhuis, Á. S. Cacciatore, R. Oldenkamp, M. S. van Ruiten, L. Willems, H. Teunissen, K. W. Muir, E. de Wit, B. D. Rowland, D. Panne, The structural basis for cohesin–CTCF-anchored loops. *Nature*. **578**, 472–476 (2020).

13. F. Jin, Y. Li, J. R. Dixon, S. Selvaraj, Z. Ye, A. Y. Lee, C.-A. Yen, A. D. Schmitt, C. A. Espinoza, B. Ren, A high-resolution map of the three-dimensional chromatin interactome in human cells. *Nature*. **503**, 290–294 (2013).

14. B. Gel, A. Díez-Villanueva, E. Serra, M. Buschbeck, M. A. Peinado, R. Malinverni, regioneR: an R/Bioconductor package for the association analysis of genomic regions based on permutation tests. *Bioinformatics*. **32**, 289–291 (2016).

15. A. S. Weintraub, C. H. Li, A. V. Zamudio, A. A. Sigova, N. M. Hannett, D. S. Day, B. J. Abraham, M. A. Cohen, B. Nabet, D. L. Buckley, Y. E. Guo, D. Hnisz, R. Jaenisch, J. E. Bradner, N. S. Gray, R. A. Young, YY1 Is a Structural Regulator of Enhancer-Promoter Loops. *Cell*. **171**, 1573-1588.e28 (2017).

16. K. D. Sullivan, M. D. Galbraith, Z. Andrysik, J. M. Espinosa, Mechanisms of transcriptional regulation by p53. *Cell Death Differ*. **25**, 133–143 (2018).

17. M. Karin, Z. Liu, E. Zandi, AP-1 function and regulation. *Curr Opin Cell Biol*. **9**, 240–246 (1997).

18. G. Wutz, C. Várnai, K. Nagasaka, D. A. Cisneros, R. R. Stocsits, W. Tang, S. Schoenfelder, G. Jessberger, M. Muhar, M. J. Hossain, N. Walther, B. Koch, M. Kueblbeck, J. Ellenberg, J. Zuber, P. Fraser, J. Peters, Topologically associating domains and chromatin loops depend on cohesin and are regulated by CTCF, WAPL, and PDS5 proteins. *Embo J*. **36**, 3573–3599 (2017).

19. B. J. Beliveau, N. Apostolopoulos, C. Wu, *Curr Protoc Mol Biology*, in press, doi:10.1002/0471142727.mb1423s105.

20. İ. A. Ilik, M. Malszycki, A. K. Lübke, C. Schade, D. Meierhofer, T. Aktaş, SON and SRRM2 are essential for nuclear speckle formation. *eLife*. **9**, e60579 (2020).

21. S. H. Ahanger, R. N. Delgado, E. Gil, M. A. Cole, J. Zhao, S. J. Hong, A. R. Kriegstein, T. J. Nowakowski, A. A. Pollen, D. A. Lim, Distinct nuclear compartment-associated genome architecture in the developing mammalian brain. *Nat Neurosci*. **24**, 1235–1242 (2021).

22. J.-H. Su, P. Zheng, S. S. Kinrot, B. Bintu, X. Zhuang, Genome-Scale Imaging of the 3D Organization and Transcriptional Activity of Chromatin. *Cell*. **182**, 1641-1659.e26 (2020).

23. E. M. Pugacheva, N. Kubo, D. Loukinov, M. Tajmul, S. Kang, A. L. Kovalchuk, A. V. Strunnikov, G. E. Zentner, B. Ren, V. V. Lobanenkov, CTCF mediates chromatin looping via N-terminal domain-dependent cohesin retention. *P Natl Acad Sci Usa*. **117**, 2020–2031 (2020).

24. A. S. Hansen, I. Pustova, C. Cattoglio, R. Tjian, X. Darzacq, CTCF and Cohesin Regulate Chromatin Loop Stability with Distinct Dynamics. *bioRxiv*, 093476 (2016).

25. R. Ciosk, M. Shirayama, A. Shevchenko, T. Tanaka, A. Toth, A. Shevchenko, K. Nasmyth, Cohesin's Binding to Chromosomes Depends on a Separate Complex Consisting of Scc2 and Scc4 Proteins. *Mol. Cell*. **5**, 243–254 (2000).

26. M. Sun, T. Nishino, J. F. Marko, The SMC1-SMC3 cohesin heterodimer structures DNA through supercoiling-dependent loop formation. *Nucleic Acids Res.* **41**, 6149–6160 (2013).

27. P. J. H. in ’t Veld, F. Herzog, R. Ladurner, I. F. Davidson, S. Piric, E. Kreidl, V. Bhaskara, R. Aebersold, J.-M. Peters, Characterization of a DNA exit gate in the human cohesin ring. *Science*. **346**, 968–972 (2014).

28. J. H. I. Haarhuis, R. H. van der Weide, V. A. Blomen, K. D. Flach, H. Teunissen, L. Willems, T. R. Brummelkamp, B. D. Rowland, E. de Wit, A Mediator-cohesin axis controls heterochromatin domain formation. *Nat Commun*. **13**, 754 (2022).

29. S. A. Quinodoz, J. W. Jachowicz, P. Bhat, N. Ollikainen, A. K. Banerjee, I. N. Goronzy, M. R. Blanco, P. Chovanec, A. Chow, Y. Markaki, J. Thai, K. Plath, M. Guttman, RNA promotes the formation of spatial compartments in the nucleus. *Cell*. **184**, 5775-5790.e30 (2021).

30. D. P. Lee, W. L. W. Tan, C. G. Anene-Nzelu, C. J. M. Lee, P. Y. Li, T. D. A. Luu, C. X. Chan, Z. Tiang, S. L. Ng, X. Huang, M. Efthymios, M. I. Autio, J. Jiang, M. J. Fullwood, S. Prabhakar, E. L. Aiden, R. S.-Y. Foo, Robust CTCF-Based Chromatin Architecture Underpins Epigenetic Changes in the Heart Failure Stress–Gene Response. *Circulation*. **139**, 1937–1956 (2019).

31. J. A. Horsfield, Full circle: a brief history of cohesin and the regulation of gene expression. *Febs J*. **290**, 1670–1687 (2023).

32. S. Cuartero, F. D. Weiss, G. Dharmalingam, Y. Guo, E. Ing-Simmons, S. Masella, I. Robles-Rebollo, X. Xiao, Y.-F. Wang, I. Barozzi, D. Djeghloul, M. T. Amano, H. Niskanen, E. Petretto, R. D. Dowell, K. Tachibana, M. U. Kaikkonen, K. A. Nasmyth, B. Lenhard, G. Natoli, A. G. Fisher, M. Merkenschlager, Control of inducible gene expression links cohesin to hematopoietic progenitor self-renewal and differentiation. *Nat. Immunol.* **19**, 932–941 (2018).

33. J. M. Moore, N. A. Rabaia, L. E. Smith, S. Fagerlie, K. Gurley, D. Loukinov, C. M. Disteche, S. J. Collins, C. J. Kemp, V. V. Lobanenkov, G. N. Filippova, Loss of Maternal CTCF Is Associated with Peri-Implantation Lethality of Ctcf Null Embryos. *Plos One*. **7**, e34915 (2012).

34. M. Gomez-Velazquez, C. Badia-Careaga, A. V. Lechuga-Vieco, R. Nieto-Arellano, J. J. Tena, I. Rollan, A. Alvarez, C. Torroja, E. F. Caceres, A. R. Roy, N. Galjart, P. Delgado-Olguin, F. Sanchez-Cabo, J. A. Enriquez, J. L. Gomez-Skarmeta, M. Manzanares, CTCF counter-regulates cardiomyocyte development and maturation programs in the embryonic heart. *Plos Genet*. **13**, e1006985 (2017).

35. R. P. Birkenbihl, S. Subramani, Cloning and characterization of rad21 an essential gene of Schizosaccharomyces pombe involved in DNA double-strand-break repair. *Nucleic Acids Res*. **20**, 6605–6611 (1992).

36. S. S. P. Rao, S.-C. Huang, B. G. S. Hilaire, J. M. Engreitz, E. M. Perez, K.-R. Kieffer-Kwon, A. L. Sanborn, S. E. Johnstone, G. D. Bascom, I. D. Bochkov, X. Huang, M. S. Shamim, J. Shin, D. Turner, Z. Ye, A. D. Omer, J. T. Robinson, T. Schlick, B. E. Bernstein, R. Casellas, E. S. Lander, E. L. Aiden, Cohesin Loss Eliminates All Loop Domains. *Cell*. **171**, 305-320.e24 (2017).

37. E. P. Nora, A. Goloborodko, A.-L. Valton, J. H. Gibcus, A. Uebersohn, N. Abdennur, J. Dekker, L. A. Mirny, B. G. Bruneau, Targeted Degradation of CTCF Decouples Local Insulation of Chromosome Domains from Genomic Compartmentalization. *Cell*. **169**, 930-944.e22 (2017).

38. J. Hyle, Y. Zhang, S. Wright, B. Xu, Y. Shao, J. Easton, L. Tian, R. Feng, P. Xu, C. Li, Acute depletion of CTCF directly affects MYC regulation through loss of enhancer–promoter looping. *Nucleic Acids Res*. **47**, 6699–6713 (2019).

39. K. Richter, M. Haslbeck, J. Buchner, The Heat Shock Response: Life on the Verge of Death. *Mol. Cell*. **40**, 253–266 (2010).

40. M. I. Love, W. Huber, S. Anders, Moderated estimation of fold change and dispersion for RNA-seq data with DESeq2. *Genome Biol.* **15**, 550 (2014).

41. M. A. Deardorff, J. J. Wilde, M. Albrecht, E. Dickinson, S. Tennstedt, D. Braunholz, M. Mönnich, Y. Yan, W. Xu, M. C. Gil-Rodríguez, D. Clark, H. Hakonarson, S. Halbach, L. D. Michelis, A. Rampuria, E. Rossier, S. Spranger, L. V. Maldergem, S. A. Lynch, G. Gillessen-Kaesbach, H.-J. Lüdecke, R. G. Ramsay, M. J. McKay, I. D. Krantz, H. Xu, J. A. Horsfield, F. J. Kaiser, RAD21 mutations cause a human cohesinopathy. *Am J Hum Genet*. **90**, 1014–27 (2012).

42. G. Borck, M. Zarhrate, J.-P. Bonnefont, A. Munnich, V. Cormier-Daire, L. Colleaux, Incidence and clinical features of X-linked Cornelia de Lange syndrome due toSMC1L1 mutations. *Hum. Mutat.* **28**, 205–206 (2007).

43. L. A. Gillis, J. McCallum, M. Kaur, C. DeScipio, D. Yaeger, A. Mariani, A. D. Kline, H. Li, M. Devoto, L. G. Jackson, I. D. Krantz, NIPBL Mutational Analysis in 120 Individuals with Cornelia de Lange Syndrome and Evaluation of Genotype-Phenotype Correlations. *Am J Hum Genetics*. **75**, 610–623 (2004).

44. A. D. Kline, J. F. Moss, A. Selicorni, A.-M. Bisgaard, M. A. Deardorff, P. M. Gillett, S. L. Ishman, L. M. Kerr, A. V. Levin, P. A. Mulder, F. J. Ramos, J. Wierzba, P. F. Ajmone, D. Axtell, N. Blagowidow, A. Cereda, A. Costantino, V. Cormier-Daire, D. FitzPatrick, M. Grados, L. Groves, W. Guthrie, S. Huisman, F. J. Kaiser, G. Koekkoek, M. Levis, M. Mariani, J. P. McCleery, L. A. Menke, A. Metrena, J. O'Connor, C. Oliver, J. Pie, S. Piening, C. J. Potter, A. L. Quaglio, E. Redeker, D. Richman, C. Rigamonti, A. Shi, Z. Tümer, I. D. C. V. Balkom, R. C. Hennekam, Diagnosis and management of Cornelia de Lange syndrome: first international consensus statement. *Nat Rev Genetics*. **19**, 649–666 (2018).

45. M. Kaur, C. DeScipio, J. McCallum, D. Yaeger, M. Devoto, L. G. Jackson, N. B. Spinner, I. D. Krantz, Precocious sister chromatid separation (PSCS) in Cornelia de Lange syndrome. *Am J Med Genet A*. **138A**, 27–31 (2005).

46. M. G. Vrouwe, E. Elghalbzouri-Maghrani, M. Meijers, P. Schouten, B. C. Godthelp, Z. A. Bhuiyan, E. J. Redeker, M. M. Mannens, L. H. F. Mullenders, A. Pastink, F. Darroudi, Increased DNA damage sensitivity of Cornelia de Lange syndrome cells: evidence for impaired recombinational repair. *Hum Mol Genet*. **16**, 1478–1487 (2007).

47. S. Kervestin, A. Jacobson, NMD: a multifaceted response to premature translational termination. *Nat. Rev. Mol. Cell Biol.* **13**, 700–712 (2012).

48. M. Haase, G. Fitze, HSP90AB1: Helping the good and the bad. *Gene*. **575**, 171–186 (2016).

49. M. L. Whitfield, L.-X. Zheng, A. Baldwin, T. Ohta, M. M. Hurt, W. F. Marzluff, Stem-Loop Binding Protein, the Protein That Binds the 3′ End of Histone mRNA, Is Cell Cycle Regulated by Both Translational and Posttranslational Mechanisms. *Mol. Cell. Biol.* **20**, 4188–4198 (2000).

50. S. Hu, P. Lv, Z. Yan, B. Wen, Disruption of nuclear speckles reduces chromatin interactions in active compartments. *Epigenetics Chromatin*. **12**, 43 (2019).

51. J.-H. Kim, D. N. Shinde, M. R. F. Reijnders, N. S. Hauser, R. L. Belmonte, G. R. Wilson, D. G. M. Bosch, P. A. Bubulya, V. Shashi, S. Petrovski, J. K. Stone, E. Y. Park, J. A. Veltman, M. Sinnema, C. T. R. M. Stumpel, J. M. Draaisma, J. Nicolai, U. of W. C. for M. Genomics, H. G. Yntema, K. Lindstrom, B. B. A. de Vries, T. Jewett, S. L. Santoro, J. Vogt, D. D. D. Study, K. K. Bachman, A. H. Seeley, A. Krokosky, C. Turner, L. Rohena, M. Hempel, F. Kortüm, D. Lessel, A. Neu, T. M. Strom, D. Wieczorek, N. Bramswig, F. A. Laccone, J. Behunova, H. Rehder, C. T. Gordon, M. Rio, S. Romana, S. Tang, D. El-Khechen, M. T. Cho, K. McWalter, G. Douglas, B. Baskin, A. Begtrup, T. Funari, K. Schoch, A. P. A. Stegmann, S. J. C. Stevens, D.-E. Zhang, D. Traver, X. Yao, D. G. MacArthur, H. G. Brunner, G. M. Mancini, R. M. Myers, L. B. Owen, S.-T. Lim, D. L. Stachura, L. E. L. M. Vissers, E.-Y. E. Ahn, De Novo Mutations in SON Disrupt RNA Splicing of Genes Essential for Brain Development and Metabolism, Causing an Intellectual-Disability Syndrome. *Am. J. Hum. Genet.* **99**, 711–719 (2016).

52. S. Cuinat, M. Nizon, B. Isidor, A. Stegmann, R. H. van Jaarsveld, K. L. van Gassen, J. J. van der Smagt, C. M. L. Volker-Touw, S. J. B. Holwerda, P. A. Terhal, S. Schuhmann, G. Vasileiou, M. Khalifa, A. A. Nugud, H. Yasaei, L. B. Ousager, C. Brasch-Andersen, W. Deb, T. Besnard, M. E. H. Simon, K. H. Amsterdam, N. E. Verbeek, D. Matalon, N. Dykzeul, S. White, E. Spiteri, K. Devriendt, A. Boogaerts, M. Willemsen, H. G. Brunner, M. Sinnema, B. B. A. D. Vries, E. H. Gerkes, R. Pfundt, K. Izumi, I. D. Krantz, Z. L. Xu, J. R. Murrell, I. Valenzuela, I. Cusco, E. Rovira-Moreno, Y. Yang, V. Bizaoui, O. Patat, L. Faivre, F. Tran-Mau-Them, A. Vitobello, A.-S. Denommé-Pichon, C. Philippe, S. Bezieau, B. Cogné, Loss-of-function variants in SRRM2 cause a neurodevelopmental disorder. *Genet. Med.* **24**, 1774–1780 (2022).

Figure legends

Figure1. CTCF and cohesin colocalize with speckle associated regions genomically.

A. Pairwise Spearman correlation between ChIP-seq signal of designated factors or histone modifications with SON-TSA seq, in IMR90 cells.
B. Example signal tracks of SON-TSA seq and ChIP-seq of designated factors, histone modifications and RNA-seq, in IMR90 cells.
C. The significance of enrichment of specific factors' genomic binding sites within speckle-associated regions was assessed using permutation analysis. In the graph, the cyan shaded region under the curve represents the distribution of SON-TSA seq signal from 1000 randomly selected regions across the genome. The black dashed line indicates the median SON-TSA seq signal of all randomly selected regions. The red shaded fraction corresponds to the area with a significance level of $p<0.05$. The solid green line represents the median value of SON-TSA seq signal from all genomic binding sites of the designated factors. SON-TSA seq data from IMR90.
D. Summary of permutation analysis results of designated factors in different cell-types.

Figure2. CTCF depletion leads to dissociation between chromatin and nuclear speckle.

A. Representative ImmunoDNA-FISH images with DAPI stained nuclei (blue), immunofluorescence of nuclear speckle component SON (green), and DNA probes targeting designated genes(red).
B. Quantification of gene loci distance to nearest nuclear speckle upon DMSO (green) or auxin (red) treatment in CTCF-AID HeLa cell lines. All box plots show the median (center line), 1.5 times the interquartile range (whiskers), and the first and third quartiles (lower and upper hinges). Data points outside the first and third quartile range are displayed as outliers. Genes are ranked based on their proximity to the nuclear speckle.
C. SON Cut&Run and CTCF ChIP-seq tracks under designated treatment at three representative genomic regions, in HeLa or IMR90 cells.
D. SON Cut&Run track for genes with corresponding DNA-FISH results shown B. The scales for all tracks range from 0-0.5, all window sizes are set to 500kb.
E. Metagene plot and heatmap of IGG normalized SON Cut&Run signal across speckle associated domains (SPADs) in CTCF-AID HeLa cells with DMSO or 24hr auxin mediated knockdown of CTCF.
F. Metagene plot and heatmap of IGG normalized SON Cut&Run signal at speckle associated domains (SPADs) in IMR90 cells, with 48hr siRNA knockdown of CTCF or negative control.
G. Metagene plot and heatmap of SON Cut&Run signal across all CTCF binding sites in IMR90 cells, with 48hr siRNA knockdown of CTCF or negative control.
H. Metagene plot and heatmap of SON Cut&Tag signal across call CTCF binding sites in K562 cells, with or without 32hr HaloPROTAC3 mediated knockdown of CTCF.

FigureS1. Quality control of CTCF depletion experiments.

A. Western blot against CTCF in CTCF-AID HeLa cells, at different timepoints after auxin treatment. M represents marker.
B. Immunofluorescence against CTCF-eGFP (green) at different timepoints after auxin treatment.
C. Morphological traits of nuclear speckles measured from Immunofluorescence against speckle marker SON, at designated timepoints after auxin treatment.

D. Correlation between SON TSA-seq and SON Cut&Run signal over all CDS across genome in IMR90 cells.
E. Correlation between nuclear speckle proximity measured by SON Cut&Run and MER-FISH in IMR90 cells.
F. Correlation between all nuclear speckle proximity data measured by DNA-FISH and SON Cut&Run under same condition in this study.
G. Whole chromosome 1 view of SON Cut&Run data under designated treatment conditions.

Figure3. CTCF-cohesin interaction is essential for chromatin-nuclear speckle association.

A. Quantification of the distance between UTP18 gene loci and the nearest nuclear speckle in CTCF-AID HeLa cells under DMSO (green) or auxin (red) treatment with designated CTCF constructs transfection. WT: whole length CTCF, NTD: N-terminal deletion, CTD: C-terminal deletion.
B. Quantification of the distance between POLH gene loci and the nearest nuclear speckle in CTCF-AID HeLa cells under DMSO (green) or auxin (red) treatment with designated CTCF constructs transfection.
C. Quantification of gene loci distance to nearest nuclear speckle upon 1hr DMSO (green) or auxin (red) treatment in Rad21-AID HeLa cells.
D. SON Cut&Run signal tracks under designated treatment at four representative genomic regions.
E. Metagene plot and heatmap of IGG normalized SON Cut&Run signal at speckle associated domains (SPADs) in Rad21-AID HeLa cells with DMSO or 1hr auxin mediated knockdown of RAD21.
F. Quantification of UTP18 gene loci distance to closest nuclear speckle upon siRNA knockdown of different cohesin pathway factors, and corresponding SON Cut&Run track with or without siRNA mediated WAPL KD.
G. Quantification of KCTD20 gene loci distance to closest nuclear speckle upon siRNA knockdown of different cohesin pathway factors, and corresponding SON Cut&Run track with or without siRNA mediated WAPL KD.
H. Metagene plot and heatmap of IGG normalized SON Cut&Run signal at speckle associated domains (SPADs), called in control HeLa cells, in HeLa cells with or without siRNA knockdown of WAPL.
I. Comparison of SPAD sizes in megabases between HeLa cells with or without siRNA knockdown of WAPL.
J. SON Cut&Run and SPADs at three representative genomic regions in HeLa cells with or without siRNA knockdown of WAPL.

FigureS2. Quality control of Rad21 depletion experiments.

A. Western blot against Rad21 in Rad21-AID HeLa cells, at different timepoints after auxin treatment. M represents marker.
B. Immunofluorescence against Rad21-eGFP (green) at different timepoints after auxin treatment.
C. Morphological traits of nuclear speckles measured from Immunofluorescence against speckle marker SON, at different timepoints after auxin treatment in Rad21-AID HeLa cells.
D. Whole chromosome 1 and 2 view of SON Cut&Run data in Rad21-AID cells with or without auxin treatment for 1hr.

E. Whole chromosome 5 view of SON Cut&Run data in HeLa cells with siRNA against WAPL or negative control for 48hr.
F. Metagene plot and heatmap of IGG normalized SON Cut&Run signal at speckle associated domains (SPADs) called in WAPL KD cells, in HeLa cells with or without siRNA knockdown of WAPL.

Figure4. Disruption of nuclear speckle association hinders the induction of nuclear speckle proximal genes.

A. Gene ontology (GO) categories enriched in nuclear speckle proximal genes in both IMR90 and HeLa cells.
B. Log2 fold change between HeLa CTCF-AID cells with or without auxin mediated CTCF depletion for 24hr. Genes are binned according to their speckle proximity, calculated from SON Cut&Run signal over CDS.
C. Log2 fold change between HeLa Rad21-AID cells with or without auxin mediated Rad21 depletion for 1hr. Genes are binned according to their speckle proximity, calculated from SON Cut&Run signal over CDS.
D. Differential conditional effect between auxin induced CTCF KD and DMSO treated HeLa cells under heat shock. Genes with significant conditional effect differences ($p<0.05$) were categorized into three bins based on nuclear speckle proximity. Left: Differential conditional effect represented by DeSeq2 calculated Log2 fold change. Right: Percentage of genes showing significantly higher (green) or lower conditional effect under heat shock.
E. Differential conditional effects of genes with significantly different SON binding in auxin induced CTCF KD vs. DMSO treated control: Genes with reduced SON signal are labeled 'away,' those with increased signal are labeled 'closer,' and genes with insignificant signal changes are labeled 'ns'.
F. Percentage of genes showing significantly higher (green) or lower conditional effect under heat shock, grouped by change in speckle proximity.
G. Representative genes with significantly differential SON binding under auxin induced CTCF KD. Box plots represent RNA-seq normalized counts. In the SON Cut&Run track, the red arrow indicates the gene CDS location, and the blocks underneath each track represent differential regions with preferential SON binding under the designated condition.
H. Differential conditional effect between siRNA mediated CTCF KD and control IMR90 cells under nutlin-3a treatment.
I. Differential conditional effects of genes with significantly different SON binding in siRNA mediated CTCF KD and control IMR90 cells.
J. Percentage of genes showing significantly higher (green) or lower conditional effect under nutlin treatment, grouped by change in speckle proximity.
K. Representative genes with significantly differential SON binding under siRNA mediated CTCF KD.
L. Differential conditional effects of genes with significantly different SON binding in siRNA mediated WAPL KD and control HeLa cells.
M. Percentage of genes showing significantly higher (green) or lower conditional effect under heat shock, grouped by change in speckle proximity.

N. Representative genes with significantly differential SON binding under siRNA mediated WAPL KD in HeLa cells.
O. Schematic model illustrating how changes in nuclear speckle proximity, resulting from CTCF or cohesin disruption, lead to differential conditional effects for speckle proximal and speckle distal genes.

FigureS3. Disruption of nuclear speckle association hinders the induction of nuclear speckle proximal genes.

A. Differential expression analysis of HeLa cells with or without 24hr auxin treatment to degrade CTCF. Blue dots represent genes significantly down-regulated (Log2 fold change <0, p<0.01), red dots represent genes significantly up-regulated (Log2 fold change >0, p<0.01). DEG: deferentially expressed genes.
B. Differential expression analysis of HeLa cells with or without 1hr auxin treatment to degrade Rad21.
C. Differential expression analysis of HeLa cells with or without 48hr siRNA mediated degradation of WAPL.
D. Differential expression analysis of HeLa cells subjected to a 1-hour heat shock treatment, with or without a 24-hour auxin treatment to degrade CTCF.

Figure5. Chromatin-speckle dissociation presents in CdLS patient derived cell lines with mutation of Rad21 genes.

A. Representative images with DAPI stained nuclei (blue), immunofluorescence of nuclear speckle component SON (green), in LCL cells from healthy donors (Ctrl1, Ctrl2) and patient 561 (P561-1, P561-2).
B. SON Cut&Run tracks from designated healthy individual or patient derived LCLs at three representative genomic regions.
C. Metagene plot and heatmap of SON Cut&Run signal across speckle associated domains (SPAD) in LCLs from designated healthy individual or patient.
D. Differential conditional effect between P561 and control LCL under heat shock.
E. Differential conditional effects of genes with significantly different SON binding in P561 vs. control LCL.
F. Representative genes with significantly differential SON binding in P561 cells.
G. Schematic model: CTCF and cohesin associate genomic regions to nuclear speckle, enabling transcription factors (TFs) to bring nearby genes closer to nuclear speckle for expressional amplification upon activation.

FigureS4. Quality control and transcriptomic profiling donor derived LCLs.

A. Sanger sequencing results within Rad21 gene coding region at chr8: 117869560-117869616.
B. Normalized transcript per million (TPM) of Rad21 genes in designated healthy individual or patient derived LCLs.
C. Morphological traits of nuclear speckles measured from Immunofluorescence against speckle marker SON in designated healthy individual or patient derived LCLs.
D. Whole chromosome 1 view of SON Cut&Run data LCLs from designated individual.
E. Differential conditional effect under heat shock between two control LCLs.

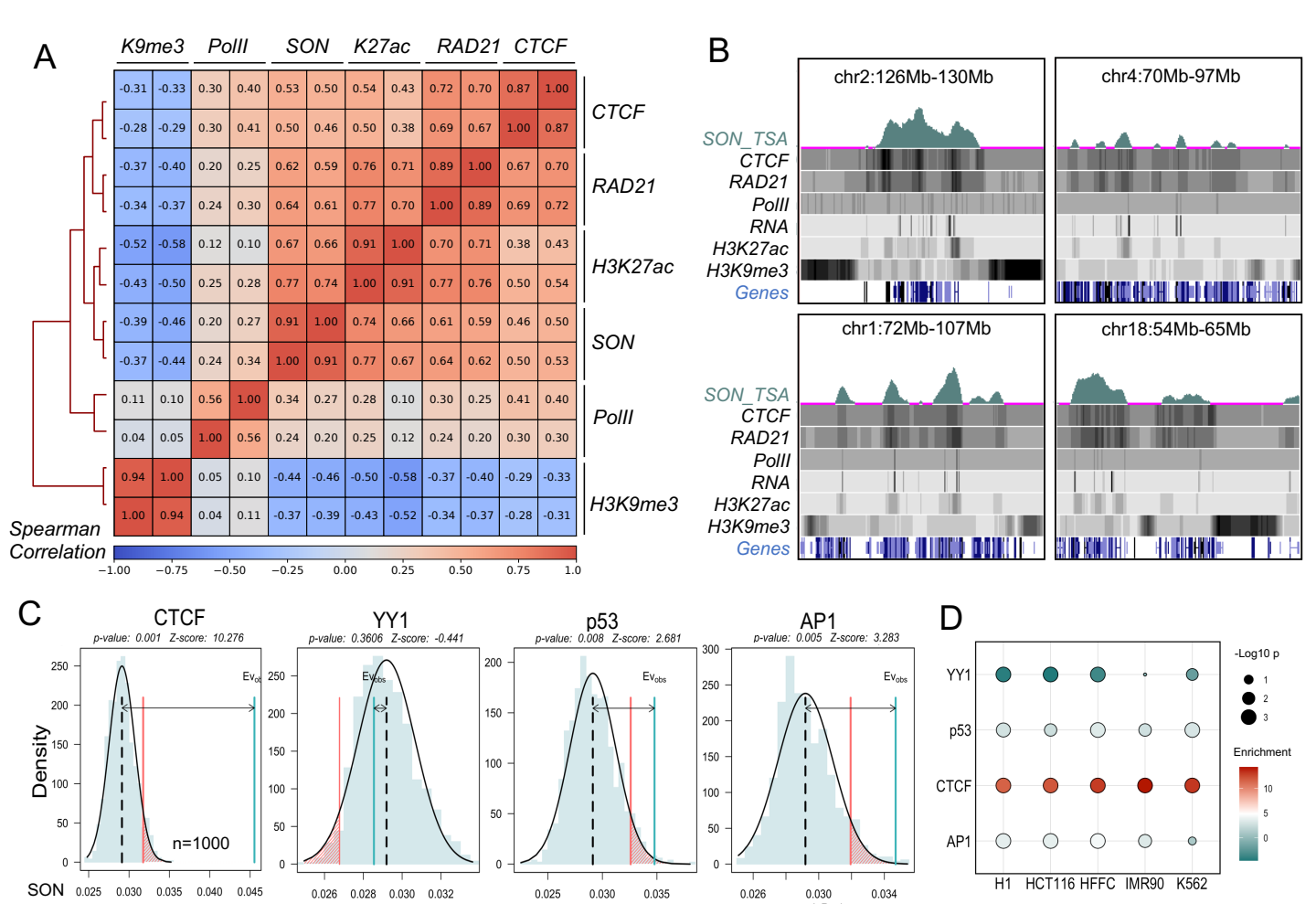
A
K9me3
PolII
SON
K27ac
RAD21
CTCF
CTCF
RAD21
H3K27ac
SON
PolII
H3K9me3
Spearman Correlation
−1.00 −0.75 −0.50 −0.25 0.00 0.25 0.50 0.75 1.0
B
chr2:126Mb-130Mb
chr4:70Mb-97Mb
chr1:72Mb-107Mb
chr18:54Mb-65Mb
SON_TSA
CTCF
RAD21
PolII
RNA
H3K27ac
H3K9me3
Genes
C
CTCF
p-value: 0.001 Z-score: 10.276
YY1
p-value: 0.3606 Z-score: -0.441
p53
p-value: 0.008 Z-score: 2.681
AP1
p-value: 0.005 Z-score: 3.283
Density
n=1000
SON
D
YY1
p53
CTCF
AP1
H1
HCT116
HFFC
IMR90
K562
-Log10 p
Enrichment

Figure1

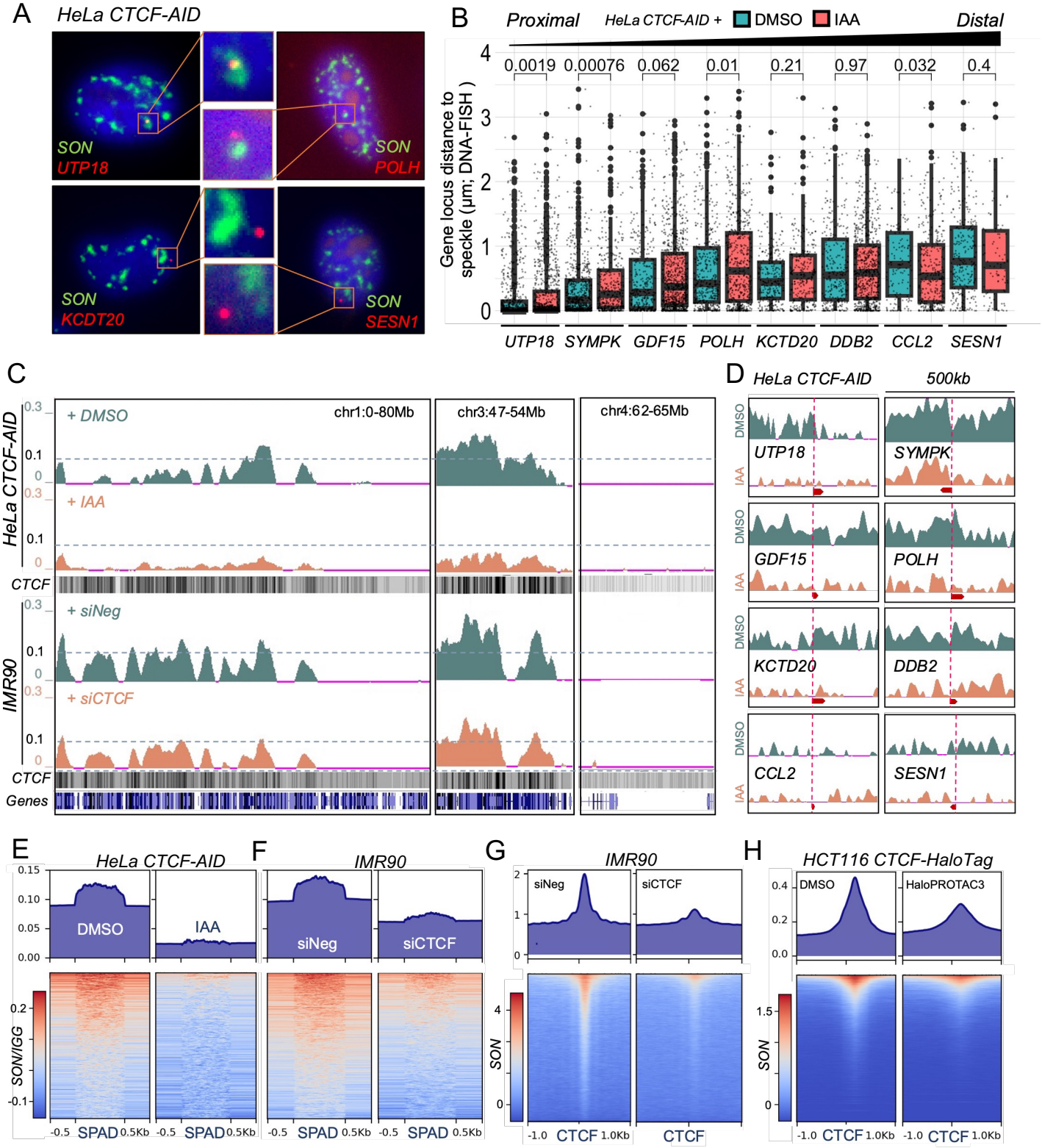
A
HeLa CTCF-AID
SON
UTP18
SON
POLH
SON
KCDT20
SON
SESN1
B
Proximal
HeLa CTCF-AID +
DMSO
IAA
Distal
0.0019
0.00076
0.062
0.01
0.21
0.97
0.032
0.4
Gene locus distance to speckle (µm; DNA-FISH)
UTP18
SYMPK
GDF15
POLH
KCTD20
DDB2
CCL2
SESN1
C
HeLa CTCF-AID
+ DMSO
+ IAA
CTCF
IMR90
+ siNeg
+ siCTCF
CTCF
Genes
chr1:0-80Mb
chr3:47-54Mb
chr4:62-65Mb
D
HeLa CTCF-AID
500kb
DMSO
IAA
UTP18
SYMPK
GDF15
POLH
KCTD20
DDB2
CCL2
SESN1
E
HeLa CTCF-AID
DMSO
IAA
SON/IGG
SPAD
F
IMR90
siNeg
siCTCF
G
IMR90
siNeg
siCTCF
SON
CTCF
H
HCT116 CTCF-HaloTag
DMSO
HaloPROTAC3
SON
CTCF

Figure2

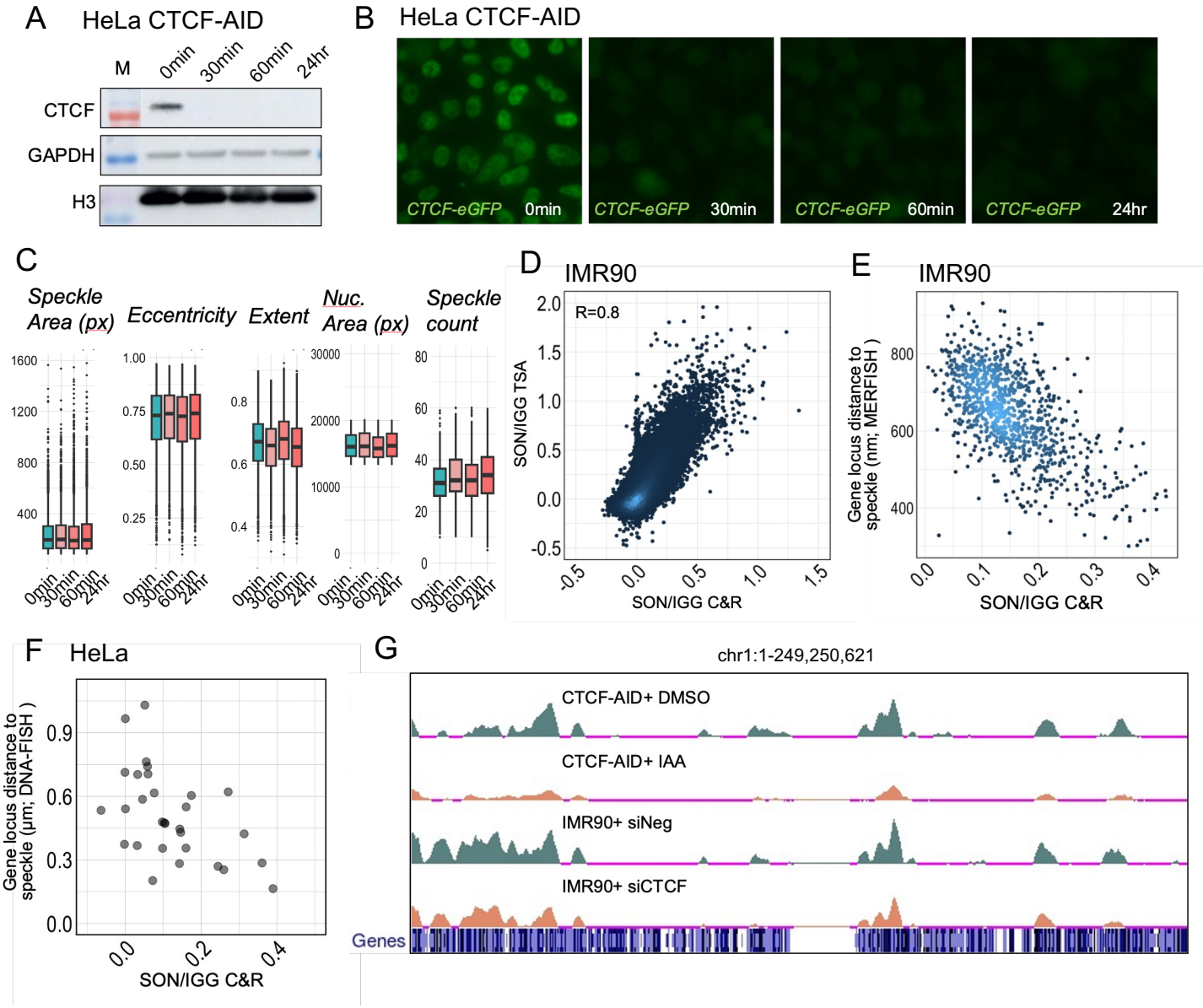
A
HeLa CTCF-AID
M
0min
30min
60min
24hr
CTCF
GAPDH
H3
B
HeLa CTCF-AID
CTCF-eGFP 0min
CTCF-eGFP 30min
CTCF-eGFP 60min
CTCF-eGFP 24hr
C
Speckle Area (px)
Eccentricity
Extent
Nuc. Area (px)
Speckle count
D
IMR90
R=0.8
SON/IGG TSA
SON/IGG C&R
E
IMR90
Gene locus distance to speckle (nm; MERFISH)
SON/IGG C&R
F
HeLa
Gene locus distance to speckle (µm; DNA-FISH)
SON/IGG C&R
G
chr1:1-249,250,621
CTCF-AID+ DMSO
CTCF-AID+ IAA
IMR90+ siNeg
IMR90+ siCTCF
Genes

FigureS1

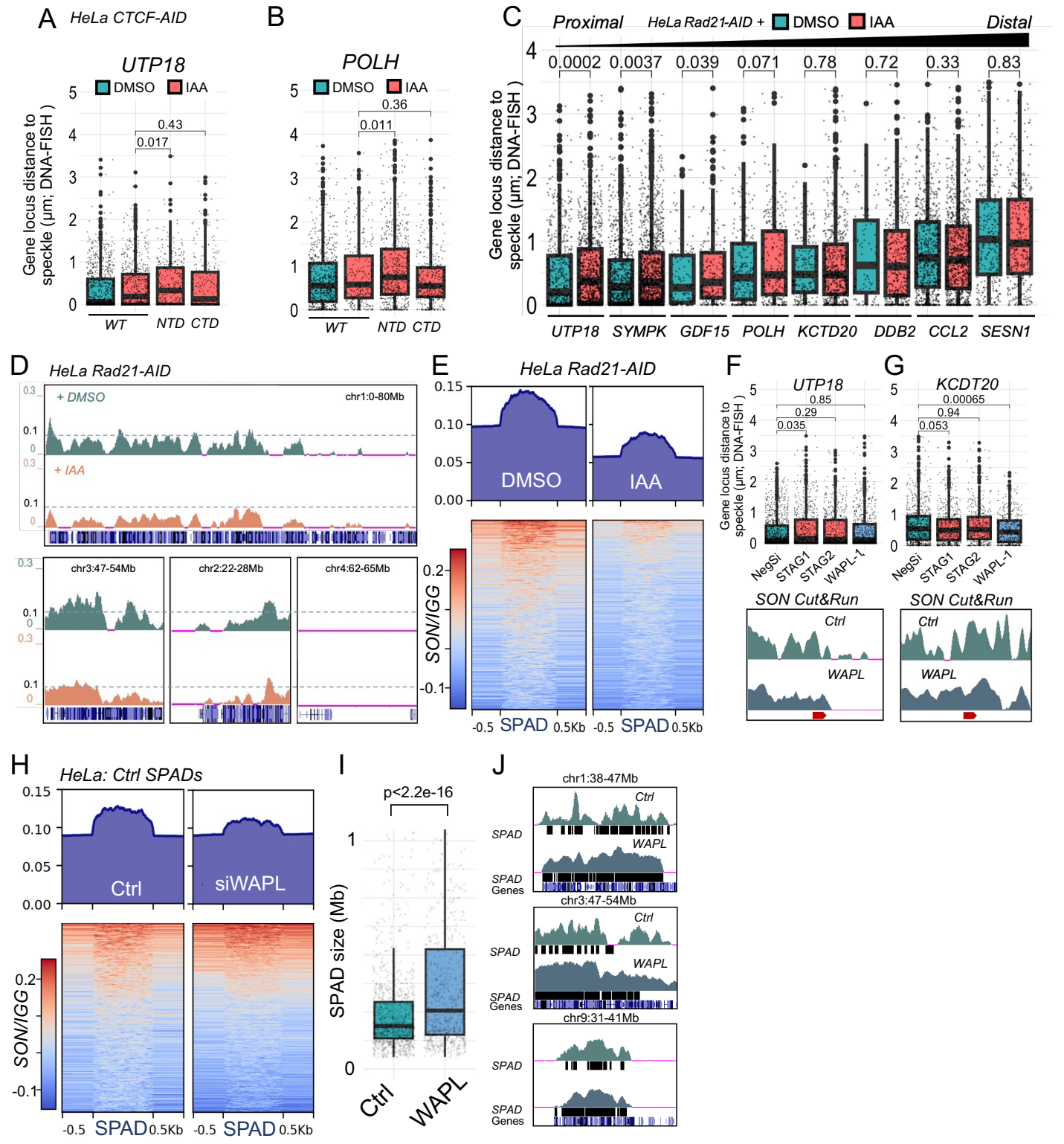
A
HeLa CTCF-AID
UTP18
DMSO
IAA
Gene locus distance to speckle (µm; DNA-FISH)
0.43
0.017
WT
NTD
CTD
B
POLH
0.36
0.011
C
Proximal
HeLa Rad21-AID +
Distal
0.0002
0.0037
0.039
0.071
0.78
0.72
0.33
0.83
UTP18
SYMPK
GDF15
POLH
KCTD20
DDB2
CCL2
SESN1
D
HeLa Rad21-AID
+ DMSO
+ IAA
chr1:0-80Mb
chr3:47-54Mb
chr2:22-28Mb
chr4:62-65Mb
E
HeLa Rad21-AID
DMSO
IAA
SON/IGG
-0.5
SPAD
0.5Kb
F
UTP18
0.85
0.29
0.035
NegSi
STAG1
STAG2
WAPL-1
SON Cut&Run
Ctrl
WAPL
G
KCDT20
0.00065
0.94
0.053
H
HeLa: Ctrl SPADs
siWAPL
I
p<2.2e-16
SPAD size (Mb)
J
chr1:38-47Mb
SPAD
SPAD Genes
chr3:47-54Mb
chr9:31-41Mb

Figure3

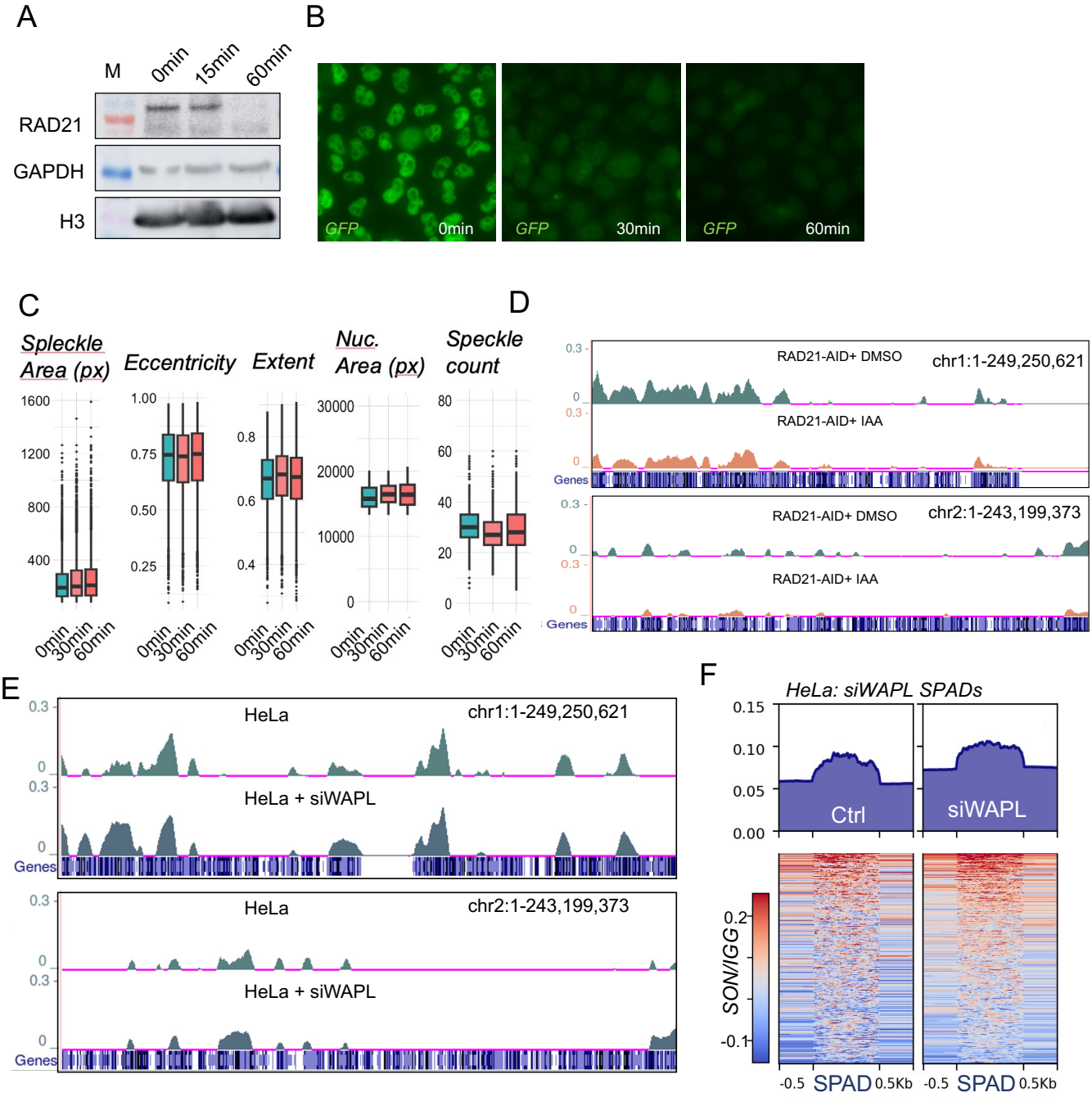
A
M
0min
15min
60min
RAD21
GAPDH
H3
B
GFP
0min
GFP
30min
GFP
60min
C
Spleckle Area (px)
Eccentricity
Extent
Nuc. Area (px)
Speckle count
0min
30min
60min
D
RAD21-AID+ DMSO
chr1:1-249,250,621
RAD21-AID+ IAA
Genes
RAD21-AID+ DMSO
chr2:1-243,199,373
RAD21-AID+ IAA
Genes
E
HeLa
chr1:1-249,250,621
HeLa + siWAPL
Genes
HeLa
chr2:1-243,199,373
HeLa + siWAPL
Genes
F
HeLa: siWAPL SPADs
Ctrl
siWAPL
SON/IGG
-0.5
SPAD
0.5Kb

FigureS2

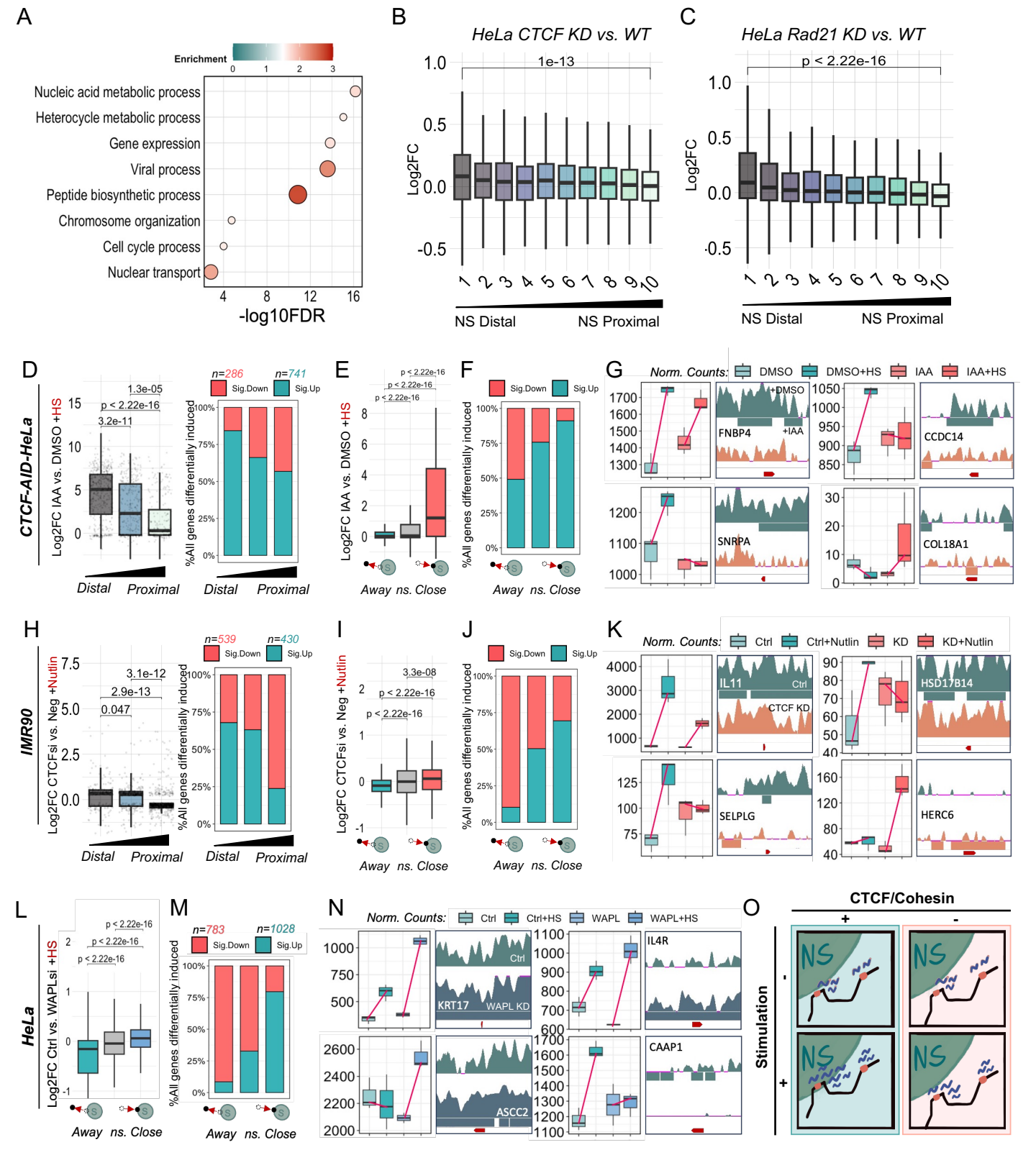
A
Enrichment
Nucleic acid metabolic process
Heterocycle metabolic process
Gene expression
Viral process
Peptide biosynthetic process
Chromosome organization
Cell cycle process
Nuclear transport
-log10FDR
B
HeLa CTCF KD vs. WT
1e-13
Log2FC
NS Distal
NS Proximal
C
HeLa Rad21 KD vs. WT
p < 2.22e-16
Log2FC
NS Distal
NS Proximal
D
CTCF-AID-HeLa
Log2FC IAA vs. DMSO +HS
1.3e-05
p < 2.22e-16
3.2e-11
Distal
Proximal
n=286
n=741
Sig.Down
Sig.Up
%All genes differentially induced
Distal
Proximal
E
Log2FC IAA vs. DMSO +HS
p < 2.22e-16
p < 2.22e-16
p < 2.22e-16
Away
ns. Close
F
Sig.Down
Sig.Up
%All genes differentially induced
Away
ns. Close
G
Norm. Counts:
DMSO
DMSO+HS
IAA
IAA+HS
FNBP4
+DMSO
+IAA
CCDC14
SNRPA
COL18A1
H
IMR90
Log2FC CTCFsi vs. Neg +Nutlin
3.1e-12
2.9e-13
0.047
Distal
Proximal
n=539
n=430
Sig.Down
Sig.Up
%All genes differentially induced
Distal
Proximal
I
Log2FC CTCFsi vs. Neg +Nutlin
3.3e-08
p < 2.22e-16
p < 2.22e-16
Away
ns. Close
J
Sig.Down
Sig.Up
%All genes differentially induced
Away
ns. Close
K
Norm. Counts:
Ctrl
Ctrl+Nutlin
KD
KD+Nutlin
IL11
Ctrl
CTCF KD
HSD17B14
SELPLG
HERC6
L
HeLa
Log2FC Ctrl vs. WAPLsi +HS
p < 2.22e-16
p < 2.22e-16
p < 2.22e-16
Away
ns. Close
M
n=783
n=1028
Sig.Down
Sig.Up
%All genes differentially induced
Away
ns. Close
N
Norm. Counts:
Ctrl
Ctrl+HS
WAPL
WAPL+HS
KRT17
Ctrl
WAPL KD
IL4R
ASCC2
CAAP1
O
CTCF/Cohesin
+
-
Stimulation
-
+
NS
NS
NS
NS

Figure4

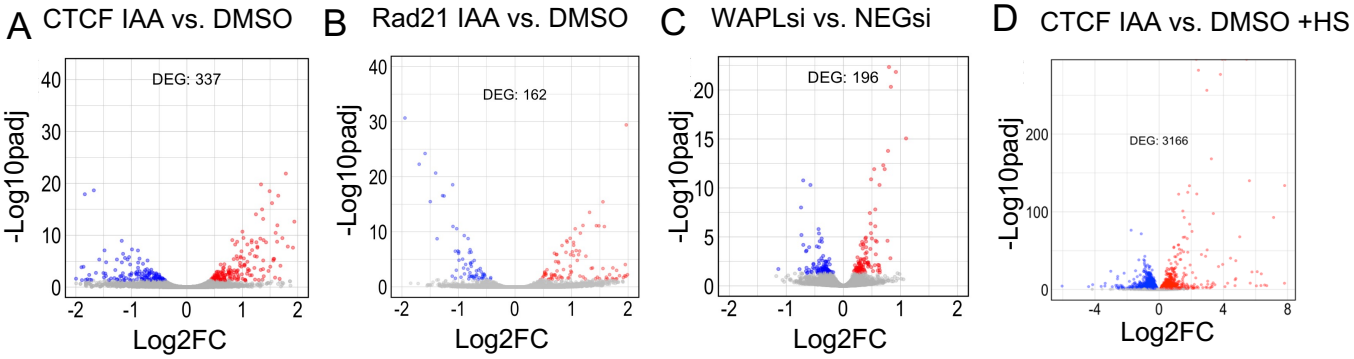
A
CTCF IAA vs. DMSO
DEG: 337
-Log10padj
Log2FC
B
Rad21 IAA vs. DMSO
DEG: 162
-Log10padj
Log2FC
C
WAPLsi vs. NEGsi
DEG: 196
-Log10padj
Log2FC
D
CTCF IAA vs. DMSO +HS
DEG: 3166
-Log10padj
Log2FC

FigureS3

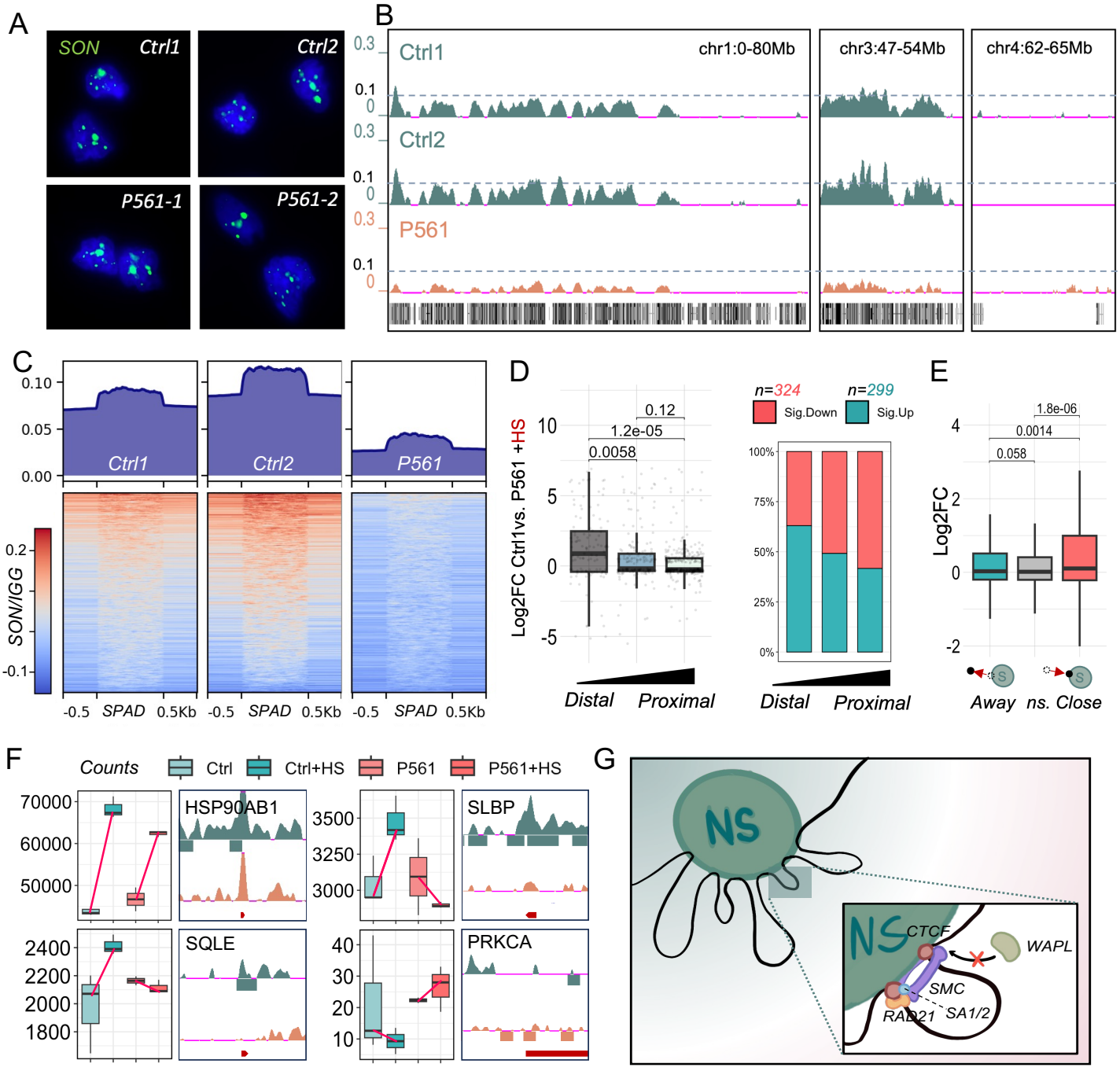
A
SON
Ctrl1
Ctrl2
P561-1
P561-2
B
Ctrl1
Ctrl2
P561
chr1:0-80Mb
chr3:47-54Mb
chr4:62-65Mb
C
Ctrl1
Ctrl2
P561
SON/IGG
-0.5 SPAD 0.5Kb
D
Log2FC Ctrl1vs. P561 +HS
0.12
1.2e-05
0.0058
Distal
Proximal
n=324
n=299
Sig.Down
Sig.Up
E
Log2FC
1.8e-06
0.0014
0.058
Away
ns.
Close
F
Counts
Ctrl
Ctrl+HS
P561
P561+HS
HSP90AB1
SLBP
SQLE
PRKCA
G
NS
CTCF
WAPL
SMC
RAD21
SA1/2

Figure5

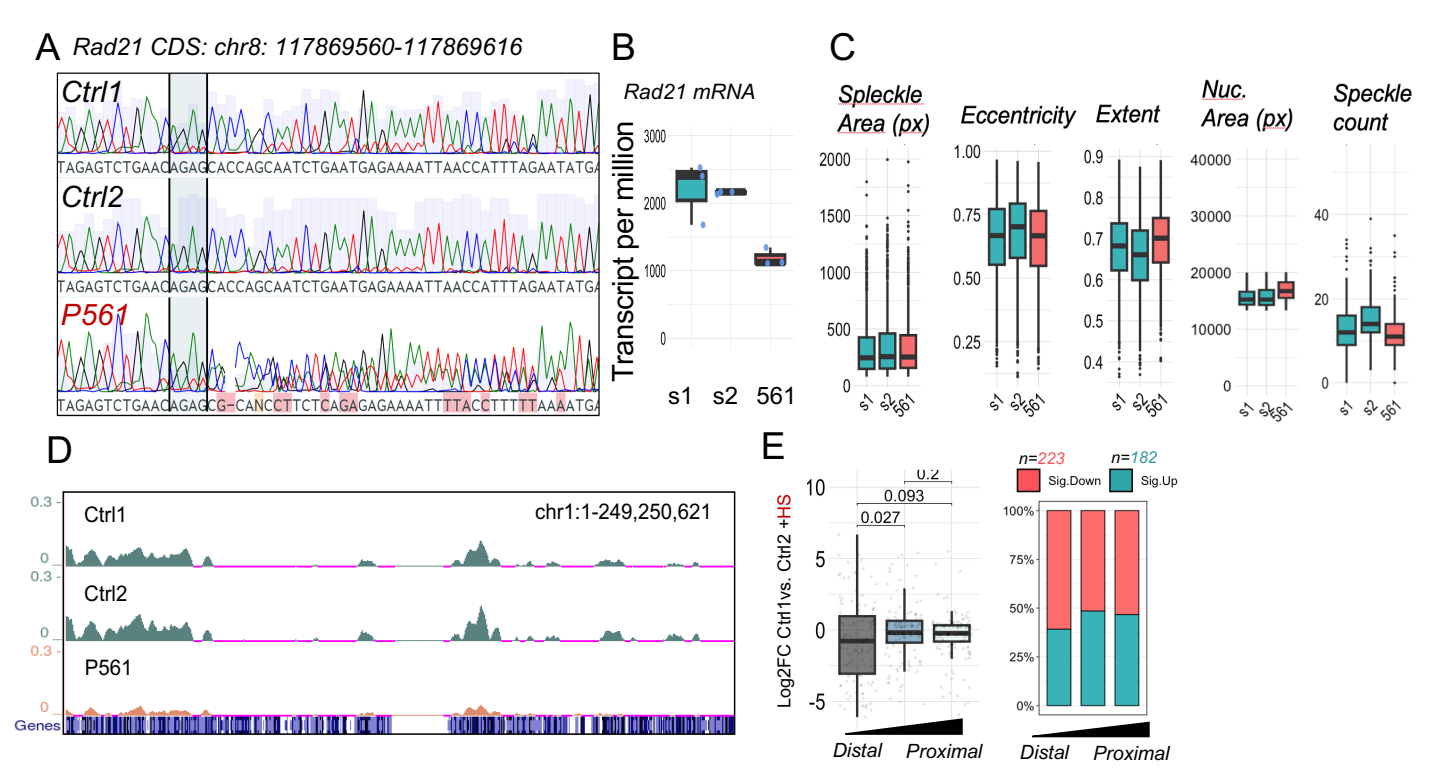
A
Rad21 CDS: chr8: 117869560-117869616
Ctrl1
Ctrl2
P561
B
Rad21 mRNA
Transcript per million
s1
s2
561
C
Spleckle Area (px)
Eccentricity
Extent
Nuc. Area (px)
Speckle count
D
Ctrl1
Ctrl2
P561
chr1:1-249,250,621
Genes
E
Log2FC Ctrl1vs. Ctrl2 +HS
0.027
0.093
0.2
Distal
Proximal
n=223
n=182
Sig.Down
Sig.Up

FigureS4